Ocean Sci. Discuss., 9, 1123–1185, 2012
www.ocean-sci-discuss.net/9/1123/2012/
doi:10.5194/osd-9-1123-2012

Ocean Science Discussions

Evaluation of real time and future global monitoring and forecasting systems at Mercator Océan

J.-M. Lellouche[1], O. Le Galloudec[1], M. Drévillon[1], C. Régnier[1], E. Greiner[2], G. Garric[1], N. Ferry[1], C. Desportes[1], C.-E. Testut[1], C. Bricaud[1], R. Bourdallé-Badie[1], B. Tranchant[2], M. Benkiran[2], Y. Drillet[1], A. Daudin[1], and C. De Nicola[1]

[1]Mercator Océan, 8/10 Rue Hermès, Ramonville Saint Agne, France
[2]CLS, 8/10 Rue Hermès, Ramonville Saint Agne, France

Received: 1 March 2012 – Accepted: 8 March 2012 – Published: 20 March 2012

Correspondence to: J. M. Lellouche (jlellouche@mercator-ocean.fr)

Published by Copernicus Publications on behalf of the European Geosciences Union.

Abstract

Since December 2010, the global analysis and forecast of the MyOcean system consists in the Mercator Océan NEMO global 1/4° configuration with a 1/12° "zoom" over the Atlantic and Mediterranean Sea. The zoom open boundaries come from the global 1/4° at 20° S and 80° N.

The data assimilation uses a reduced order Kalman filter with a 3-D multivariate modal decomposition of the forecast error. It includes an adaptative error and a localization algorithm. A 3D-Var scheme corrects for the slowly evolving large-scale biases in temperature and salinity.

Altimeter data, satellite temperature and in situ temperature and salinity vertical profiles are jointly assimilated to estimate the initial conditions for the numerical ocean forecasting.

This paper gives a description of the recent systems. The validation procedure is introduced and applied to the current and future systems. This paper shows how the validation impacts on the quality of the systems. It is shown how quality check (in situ, drifters) and data source (satellite temperature) impacts as much as the systems design (model physics and assimilation parameters). The validation demonstrates the accuracy of the MyOcean global products. Their quality is stable in time. The future systems under development still suffer from a drift. This could only be detected with a 5 yr hindcast of the systems. This emphasizes the need for continuous research efforts in the process of building future versions of MyOcean2 forecasting capacities.

1 Introduction

MyOcean, and soon its follow-on MyOcean2, is the implementation project of the GMES Marine Core Service, aiming at deploying the first concerted and integrated pan-European capacity for ocean monitoring and forecasting. Maritime security, oil spill prevention, marine resources management, climate change, seasonal forecasting, coastal

OSD
9, 1123–1185, 2012

activities, ice sheet surveys, water quality and pollution are some of the targeted applications. MyOcean service provides the best information available on the ocean for the global and regional scales based on the combination of space and in situ observations, and their assimilation into 3-D simulation models.

Scientific quality is one of the criteria that guided the continuous improvement of the MyOcean products. Moreover, scientific quality information has a strong impact on the users understanding of the products content and interest. Thus, it is important that the monitoring and forecasting centres (MFCs) agree on standards and produce homogeneous and accessible information on the scientific quality of the analysis and forecast. Some of these standards have to be common with ocean observations thematic assembly centres (TACs) in order to provide synthetic and consistent information to the final user.

The scientific assessment procedure operated during MyOcean consists in two phases. In the first "calibration phase", new products or developments are checked with a series of metrics before their operation. Once the product is operational, a "validation phase" takes place where the products are checked against the reference calibration results.

Standards and metrics have been defined during MERSEA (Marine Environment and Security for the European Area, http://www.ifremer.fr/merseaip) integrated project and in the context of GODAE (Global Ocean Data Assimilation Experiment, http://www.godae.org). Some of them have been proposed for calibration and validation purposes. The validation procedure already defined at Mercator Océan fitted well into this model, with a scientific assessment (calibration) and quarterly control bulletins (validation). Additionally, a routine check of more than a thousand diagnostics is performed every day at Mercator Océan.

Since January 2009, Mercator Océan, which is in charge of the global ocean, has developed several versions of monitoring and forecasting system for the various milestones V0, V1 and V2 of the MyOcean project (Fig. 1). The Mercator Océan monitoring and forecasting system is based on the ocean modelling platform NEMO (Nucleus

OSD
9, 1123–1185, 2012

for European Modelling of the Ocean) and the SAM (Système d'Assimilation Mercator) data assimilation system. It is declined in different configurations. The main target configuration is a global high resolution system at 1/12° horizontal resolution and 50 vertical levels. Due to its high computational cost, the major scientific advances are first implemented and tested with a global intermediate resolution system at 1/4° and 50 vertical levels (hereafter referred to as IRG). High resolution is maintained in the Atlantic and Mediterranean via the nesting of a high resolution zoom at 1/12° (hereafter referred to as HRZ).

Global MyOcean products are available on eleven regions (ocean basins) that match the inter-comparison zones defined in the context of the international GODAE Oceanview initiative. For each zone the best available product was selected for diffusion through MyOcean. The highest resolution available is provided for each zone in order to ensure the highest possible accuracy and consistency.

This article presents the main results of the scientific assessment of MyOcean V2 global MFC at Mercator Océan and shows how the validation impacts on the quality of the systems. We focus on HRZ and IRG as these are the most advanced systems in terms of scientific developments of both the physical model and the data assimilation system. The main characteristics of these monitoring and forecasting systems are described in Sect. 2. The validation methodology is detailed in Sect. 3. The main results of the scientific assessment are given in Sect. 4. For each diagnostic, the results of MyOcean V2 system (current IRG_V1V2 and HRZ_V1V2) are compared with the results from the latest versions of the systems under development (IRG_DEV and HRZ_DEV) that will be available in MyOcean2 (see Fig. 1). In Sect. 5 a summary of the scientific assessment is given, and the improvements expected for MyOcean2 in terms of performance and validation procedure are discussed.

OSD
9, 1123–1185, 2012

2 Description of the monitoring and forecasting systems

In the following, a general description of the systems is given with a focus on IRG_V1V2 and HRZ_V1V2. The main differences and links between all versions of systems are summarized in Tables 1 and 2 for all IRG and HRZ systems, respectively.

2.1 A common basis for all forecasting systems

2.1.1 Physical model

Since MyOcean V1, the IRG and HRZ systems use the version 3.1 of NEMO (Madec, 2008). "Partial cells" parameterization has been chosen for a better representation of the topographic floor (Barnier et al., 2006) and we compute the momentum advection term with the energy and enstrophy conserving scheme proposed by Arakawa and Lamb (1981). Other following options are implemented in the model configurations: the advection of the tracers (temperature and salinity) is computed with a total variance diminishing (TVD) advection scheme (Lévy et al., 2001; Cravatte et al., 2007), a free surface filtering out the high frequency gravity waves is used (Roullet and Madec, 2000), a laplacian lateral isopycnal diffusion on tracers ($300\,m^2\,s^{-1}$ for IGR, $125\,m^2\,s^{-1}$ for the HRZ at the equator and decreasing poleward, proportionally to the grid size), an horizontal biharmonic viscosity for momentum ($-1\times10^{11}m^4\,s^{-1}$ for IRG and $-1.5\times10^{10}m^4\,s^{-1}$ for the HRZ at the equator and decreasing poleward as the cube of the grid size). The vertical mixing is parameterized according to a turbulent closure model (order 1.5) adapted by Blanke and Delecluse (1993). The lateral friction condition is a partial-slip condition with a regionalization of a no-slip condition (over the Mediterranean Sea) for HRZ system. The Elastic-Viscous-Plastic rheology formulation for the LIM2 ice model (hereafter called LIM2_EVP, Fichefet and Maqueda, 1997) has been activated (Hunke and Dukowicz, 1997). The monthly runoff climatology is built from coastal runoffs and 100 major rivers from Dai and Trenberth (2002) together with an annual estimation of the Antarctica ice sheets melting given by Jacobs et al. (1992).

OSD
9, 1123–1185, 2012

Barotropic mixing due to tidal currents in the semi-enclosed Indonesian throughflow region, has been parameterized in IRG_V1V2 following Koch-Larrouy et al. (2008). Atmospheric fields are issued from the ECMWF (European Centre for Medium-Range Weather Forecasts) Integrated Forecast System. We use a 3 h sampling to reproduce the diurnal cycle, concomitant to the use of the 1 m thickness of the uppermost level and according to Bernie et al. (2005), this temporal and vertical resolution are sufficient to capture 90 % of the SST diurnal variability and the maximum heating rates of the diurnal cycle. Momentum and heat turbulent surface fluxes are computed from CORE bulk formulae (Large et al., 2009) using the usual set of atmospheric variables: surface air temperature at 2 m height, surface humidity at 2 m height, mean sea level pressure and the wind at 10 m height. Daily downward longwave and shortwave radiative fluxes and rainfalls (solid + liquid) fluxes are also used in the surface heat and freshwater budgets. An analytical formulation (Bernie et al., 2005) is applied to the shortwave flux in order to reproduce ideally the diurnal cycle.

Considering the physical model, the main improvements of the current systems (IRG_V1V2 and HRZ_V1V2) in comparison with V0 systems concern the use of high frequency (3 h) atmospheric forcings including the diurnal cycle, the use of the CORE bulk formulation instead of CLIO one (Goosse et al., 2001) and the use of the LIM2_EVP ice model (see Tables 1 and 2). The use of a one-way nesting between the systems is another improvement with respect to V0. Since V1, IRG system gives boundary conditions for HRZ system.

2.1.2 Data assimilation scheme

The SAM data assimilation method relies on a reduced order Kalman filter based on the Singular Evolutive Extended Kalman Filter (SEEK) formulation introduced by Pham et al. (1998). This approach is used for several years at Mercator Océan and has been implemented into different ocean model configurations with a 7-day assimilation window (Tranchant et al., 2008; Cummings et al., 2009). In all Mercator Océan forecasting systems, the forecast error covariance is based on the statistics of a collection of 3-D

OSD
9, 1123–1185, 2012

ocean state anomalies, typically a few hundred. This approach comes from the concept of statistical ensembles where an ensemble of anomalies is representative of the error covariances. In this way, the truncation does not take place any more, thus it is only necessary to generate the appropriate number of anomalies. This approach is similar to the Ensemble Optimal Interpolation developed by Oke et al. (2008). In our case, the anomalies are computed from a long numerical experiment (typically around 10 yr) with respect to a running mean so that they can give and estimate of the 7-day scale error on the ocean state at a given period of the year for Temperature (T), Salinity (S), zonal velocity (U), meridional velocity (V) and Sea-Surface-Height (SSH). It should also be noted that the analysis increment is a linear combination of these anomalies and depends on the innovation (observation minus model forecast equivalent) and on the specified observation errors. A particular feature of the SEEK is that the error covariance only gives the direction of the model error, not its intensity. An adaptive scheme for the model error variance has been implemented which calculates an optimal variance of the model error based on a statistical test formulated by Talagrand (1998). The last feature of the model forecast covariance employed is the use of a weighting function which sets the covariances to zero beyond a distance defined as twice the local spatial correlation scale. Because we use a finite number of ocean state anomalies to build the model forecast covariance, the latter is not significant any more away from a certain distance of the analysis point (from a statistical point of view). That is why it is preferable not to use this information and to set the covariance to zero. Spatial (zonal and meridional directions) and temporal correlation scales (Fig. 2) are then used to define an "influence bubble" around the analysis point in which data are also selected. The analysis is performed on a reduced horizontal grid (1 point every 4 in both directions) in order to reduce the computational cost. An important difference of MyOcean V2 systems with more classical forecasting system is that the analysis is not performed at the end of the assimilation window but at the middle of the 7-day assimilation cycle. The objective is to take into account information both in the past and in the future and to provide the best estimate of the ocean centred in time. Using such an approach,

OSD
9, 1123–1185, 2012

the analysis has a smoother like feature. For technical reasons, this could not be done exactly at time = 3.5 days so it has been slightly shifted at time = 4 days.

The data assimilation produces, after each analysis, increments of barotropic height, temperature, salinity and zonal and meridional velocity. A physical balance operator allows to deduce from these increments a physically consistent sea surface height increment. All these increments are applied progressively thanks to the Incremental Analysis Update (IAU) method (Bloom et al., 1996; Benkiran and Greiner, 2008) allowing to avoid model shock every week due to the unbalance between the analysis increments and the model physics.

In addition to the assimilation scheme, a method of bias correction has been developed. This method is based on a 3-D-variational approach which takes into account cumulative innovations on the later 3-month period in order to estimate large scale temperature and salinity biases when enough observations are present. The aim of the bias correction is to correct the large scale slowly varying error of the model under the thermocline whereas SAM assimilation scheme is to correct the smaller scales of the model forecast error.

The assimilated observations consist of along track altimeter Sea Level Anomalies (SLA) from AVISO, Sea-Surface-Temperature (SST) from either NCEP or NOAA, and temperature and salinity in situ vertical profiles from CORIOLIS centre. The first guess at appropriate time (FGAT) method (Huang et al., 2002) is used, which means that the model equivalent of the observation for the innovation computation is taken at the time for which the data is available, even if the analysis is delayed. The concept of "pseudo-observations" or "Observed-No-Change" (innovation equal to zero) has also been introduced to overcome the deficiencies of the background errors, in particular for extrapolated and/or poorly observed variables. We apply this kind of parameterization on the barotropic height, the variables under the ice, on coastal salinity (runoffs), at the equator on the velocities and on open boundaries (for HRZ systems only). Lastly, the Mean Dynamic Topography (MDT) named "CNES-CLS09" derived from observations and described in Rio et al. (2011) is used as a reference for SLA assimilation.

OSD
9, 1123–1185, 2012

Considering the data assimilation method, the main improvements of the current systems (IRG_V1V2 and HRZ_V1V2) in comparison with previous systems concern the insertion of the zonal and meridional velocity components into the control vector, the use of the IAU procedure, the insertion of new observational operators, the use of the CNES-CLS09 MDT, the introduction of 2-D and 3-D pseudo-observations and the use of a method of bias correction (see Tables 1 and 2).

2.2 The HRZ_V1V2 specificities

Unrealistic salinities were diagnosed by several users (coastal applications), shortly after putting HRZ_V1 system in real time. This problem appeared in the HRZ_V1 products on the continental shelves, and in particular in the Celtic Seas, the North Sea and the Bay of Biscay. An upgrade of the system, called HRZ_V1V2, was implemented in order to correct these biases and it replaced previous HRZ_V1 system starting from July 2011 (see Fig. 1). Those updates included the modification of the multivariate data assimilation in order to use an adjusted version of CNES-CLS09 MDT updated with GOCE observations and bias correction. An intermediate resolution SST at 1/4° including AVHRR and AMSRE observations (Reynolds et al., 2007), called hereafter "AVHRR + AMSRE", was also assimilated in place of RTG-SST NCEP (Gemmill et al., 2007), called hereafter "RTG". The observation error covariance was increased for the assimilation of SLA near the coast and on the shelves, and for the assimilation of SST near the coast (within 50 km off the coast). The spatial correlation radii were modified everywhere to improve particularly the analysis near the European coast. The system was restarted from October 2009 and not from October 2006, as for all the other systems, because of the computing time required to catch up with real time and the need to correct operational analyses and forecasts quickly. Temperatures and salinities were initialized with climatological conditions from Levitus 2005 (Antonov et al., 2006; Locarnini et al., 2006). Initial condition for the sea ice concentration was inferred from the IFREMER/CERSAT products (Ezraty et al., 2007) for October 2009. The sea ice thickness distribution has been directly issued from the Mercator Océan global

OSD
9, 1123–1185, 2012

1/4° reanalysis GLORYS2V1 (GLobal Ocean ReanalYsis and Simulation, Ferry et al., 2011). A monthly average (October 2009) of the sea ice field has been used, the latter having the advantage to be dynamically equilibrated after the 17 yr (1993–2009) of the reanalysis experiment.

2.3 Updates for future MyOcean versions

Current IRG_V1V2 MyOcean system is built on a physical model configuration (ORCA025) that is extensively used and regularly updated in the ocean modelling community (Barnier et al., 2006; Penduff et al., 2007, 2010; Lombard et al., 2009; Lique et al., 2011). Its operational products feed the open boundaries of the HRZ_V1V2 and give the physical forcings for the Mercator Océan biogeochemical system BIOMER (Elmoussaoui et al., 2011). However, IRG_V1V2 does not benefit from the improvements that were implemented in HRZ_V1V2 (see Sect. 2.2). To ensure consistency between Mercator Océan systems that will be operated in 2012 and to correct some deficiencies of the latter, test experiments were carried out with the following additions and changes: (1) Instead of being constant, the depth of light extinction is separated in Red-Green-Blue bands depending on the mean monthly climatology SeaWIFS chlorophyll data distribution. (2) Large scale correction have been applied to the downward (shortwave and longwave) radiative and the precipitation fluxes. This method based on satellite estimates first used on the ERA-Interim products (Garric et al., 2011) has been adapted to the ECMWF fluxes. (3) The estimation of Silva et al. (2006) has been implemented in IRG_DEV to represent the amount and distribution of meltwater attributable to giant and small icebergs calving from Antarctica in the form of a monthly climatological runoff at the southern ocean surface. (4) Despite the previous correction and updates, the freshwater budget is far from being equilibrated. In order to avoid any mean sea surface height drift and to reduce errors in the SLA assimilation, the surface mass budget is set to zero in IRG_DEV at each time step with a superimposed seasonal cycle (Chen et al., 2005). The residual surface mass budget from IRG_DEV system is evaluated over the HRZ_DEV domain and removed in the HRZ_DEV surface

OSD
9, 1123–1185, 2012

mass budget. The concentration/dilution water flux term is not set to zero. (5) As already made in HRZ_V1V2 system, AVHRR + AMSRE SST has been assimilated in IRG_DEV and HRZ_DEV, in place of RTG SST. (6) An error map based on the maximum of sea ice extent was applied to Envisat altimeter to correctly assimilate the data in the Arctic. (7) Since October 2010, Envisat altimeter is brought to a new lower orbit, which has led to a slight degradation of data quality (Ollivier and Faugere, 2010). This degradation is due to the fact that SLA is computed relatively to a Mean Sea Surface outside from the historical repeat track where the quality is lower. This is particularly true at high latitudes where no track from other missions is available. For that reason, Envisat error was increased by 2 cm over the entire domain and by 5 cm above 66° N. (8) New temperature and salinity vertical profiles from sea mammal's (elephant seals) database (Roquet et al., 2011) were assimilated to reduce the lack of such data at high latitudes. (9) A Quality Check (QC) of T/S vertical profiles has been implemented to discard suspicious temperature and salinity vertical profiles (see Sect. 3.4).

3 Scientific assessment and validation methodology

3.1 A hierarchy of metrics

The selection of a number of ocean forecast scores has been initiated with the definition of an ensemble of metrics in the context of the European MERSEA project and the international GODAE initiative. These standardized diagnostics have permitted intercomparison exercises between operational oceanography Monitoring and Forecasting Centres (MFCs) at the European (Crosnier and Le Provost, 2007) and worldwide levels (Hernandez et al., 2009).

During the MyOcean project, scientists from all MFCs and TACs have been exchanging ideas in order to define the MyOcean calibration and validation metrics depending on the region and the type of product, including observational products. The so-called "Product Quality and Calibration/Validation group" produced a large num-

OSD
9, 1123–1185, 2012

ber of diagnostics and proposed complementary methodologies (see Table 3) showing all types of metrics used for Calibration/Validation during MyOcean. Many efforts were made to synthesize and homogenise quality information in order to provide quality summaries and accuracy numbers. In the meantime, quarterly bulletins "QuO Va Dis?" have been developed at Mercator Océan as a proposition for future MyOcean quality bulletins, and validation webpages were developed by several groups in order to provide interactive quality information to the users (see for instance http://gnoo.bo.ingv.it/myocean/calval). All these rely on the same basis of metrics that can be classified in four main categories derived from Crosnier and Le Provost (2007).

The consistency between two system solutions or between a system and observations can be checked by "eyeball" verification. This consists in comparing subjectively two instantaneous spatial maps of a given quantity. Coherent spatial structures or oceanic processes such as main currents, fronts and eddies are evaluated. This process is referred to as CLASS1 metrics. The consistency in time is checked with CLASS2 metrics which include comparisons of moorings time series, and statistics between time series. Space and/or time integrated quantities such as volume and heat transports, heat content and eddy kinetic energy are referred to as CLASS3. These quantities are generally compared with literature values or values obtained with past time observations such as climatologies, or with reanalyses. Finally, CLASS4 metrics give a measure of the real time accuracy of the systems, by comparing with various statistics all available oceanic observations (in situ or satellite) with their model equivalent at the time and location of the observation.

3.2 Scientific assessment as a way to define a "standard behaviour"

Since 2008 and in preparation of MyOcean, Mercator Océan has been defining and following a rigorous integration and validation plan for the implementation of new versions of the ocean forecasting systems. This plan includes a thorough scientific assessment which gives a general picture of the standard behaviour of the system in terms of accuracy and realism of the ocean physics. The accuracy is measured with departures

OSD
9, 1123–1185, 2012

from observations and the realism by studying oceanic processes. The scientific assessment procedure involves all classes of metrics described in previous section. It controls the improvements between versions of a system, and ensures that a version is robust and its performance stable over time.

The assessment must be conducted on a one-year numerical experiment at least, in order to obtain representative results. It is currently very difficult to run the real time systems over many years in the past, for computational reasons, but also due to the recent (and ongoing) evolution of the ocean observational network. Different data densities imply different tunings of the data assimilation system. Moreover, homogeneous (reanalysed) atmospheric fluxes are needed to perform several decades' long experiments. GLORYS2V1 ocean reanalysis spans the 1993–2009 period and is the longest numerical experiment with a system close to IRG_V1V2 real time monitoring and forecasting system. The IRG_V1V2 and HRZ_V1V2 numerical experiments do not start before October 2006 which is a good compromise between computational costs needed to catch up with real time and the presence of a large enough observation networks together with high resolution atmospheric forcing from ECMWF operational forecast. The MyOcean scientific calibration phase corresponds to the scientific assessment performed at Mercator Océan. The scientific assessment results are illustrated here with diagnostics on the year 2010 mainly, assorted with time series on the 2007–2011 period.

3.3 Delayed time and real time quality check of the monitoring system

Once the scientific assessment is done, and the system and standard accuracy values and consistent behaviour are described, it is possible to apply a regular quality check to the real time analyses and forecasts. Due to the very large amount of information produced by a global system, the real time quality control is based on a reduced number of metrics, and comparisons with observations are constrained by their availability and timeliness. However, more than a thousand graphics are controlled each week (weekly control of the analysis) and each day (consistency check of the daily forecast)

OSD
9, 1123–1185, 2012

by Mercator Océan. The major part of this procedure is currently being automated with indicators based on distribution (percentiles) thresholds computed from the scientific assessment stage.

Most Numerical Weather Prediction centres publish quality reports on a regular basis which record the strengths and weaknesses of the forecasting systems, as well as the technical changes in the systems, or the spatial and temporal coverage of the input data (see for instance http://www.ecmwf.int/publications/newsletters/). Following this example, the Quarterly Ocean Validation Bulletin "QuO Va Dis?" is published by Mercator Océan since July 2010. It is available on request (qualif@mercator-oecan.fr) and written in English for the sake of MyOcean users. This quality report is meant to be a comprehensive expertise, it is still evolving towards a synthetic and easy to read format. It currently displays a synthesis of input data information including maps of the spatial coverage of the input data. The main information on data availability on the period is also reminded. A short description is made of the main large scale atmosphere and climate forcing exerted on the ocean and the large scale ocean atmosphere couplings that are taking place. Observation minus analysis (called "residual") and observation minus forecast (called "innovation") statistics are displayed for T and S vertical profiles, SST and SLA observations that are assimilated. Both 2-D maps (averages in layers) and synthetic histograms or time series (averages in one given region) are shown to give a view of the time and space variation of the system skill and of the major uncertainties. Temperature versus salinity diagrams allow us to give an oceanographic interpretation of statistics. 2-D maps of analysis minus forecast differences give an alternative view of the system skill.

Comparisons are made with observations that are not yet assimilated in the system, like high resolution SST OSTIA (Operational Sea Surface Temperature and Sea-Ice Analysis, Donlon et al., 2012) which is the global MyOcean SST product, currents at 15 m derived from drifting buoys, sea ice concentration and drift, or tide gauges (the low frequency component of the tide gauges elevation signal). Integrated quantities

OSD
9, 1123–1185, 2012

such as sea ice extent and global mean SST are monitored. Process studies focusing on one process or region, or short R&D validation studies complement the bulletins.

3.4 Quality control and feedback to input data providers

To minimise the risk of erroneous observations being assimilated in the model, the system carries out a Quality Control (QC) on the assimilated T and S vertical profiles. This is in addition to the quality control procedures performed by the data producers.

The basic hypothesis of the data assimilation system is that innovations are normally distributed in each point of the ocean (Gaussian distribution of background errors). Observations for which the innovation is in the tail of the distribution will thus be considered as questionable. Average and standard deviation of the innovations from GLORYS2V1 which characterize the normal distribution of Mercator Océan systems innovations in each point of the ocean (longitude, latitude and depth) and for each season, were used to evaluate all profiles from the CORA3.1 dataset (Cabanes et al., this issue 2012). The implementation of this QC can be summarized as follows. An observation is considered as suspect if two conditions are met. The first condition is a threshold criterion on the innovation. The second condition keeps the observation close to the climatology even if the innovation is high because the model has drifted. Figure 3 shows an example of a wrong temperature profile detected by the QC in the GLORYS2V1 simulation. From 500 m depth, innovations are no longer valid. The two conditions described previously are not satisfied and the profile is rejected (Fig. 3a). When this profile is assimilated, an abnormal value of salinity appears at the temporal and geographical positions of this profile (Fig. 3b). This is due to the fact that the assimilation algorithm used is multivariate, meaning that an observation of temperature leads to corrections of all the model variables and especially here the surface salinity.

For each year of the 1993–2009 GLORYS2V1 simulation, all questionable profiles were identified and percentages of rejection and spatial distribution of questionable observations were produced. Finally, the list of questionable observations was sent to CORIOLIS centre who in turn flagged around 50 % of these observations as bad in the

OSD
9, 1123–1185, 2012

new CORA3.2 dataset (Cabanes et al., this issue 2012), which is used by IRG_DEV and HRZ_DEV systems. MFCs will be routinely transferring an increasing number of feedbacks to TACs, at the MyOcean level but also at the international level in the context of GODAE Oceanview.

The real time counterpart of this QC of oceanic observations based on forecasting system innovations has been implemented in IRG_DEV and HRZ_DEV. The parameters (average and standard deviation of the innovations) were calculated from GLORYS2V1 which among other things assimilated the CORA3.1 database. In principle, these parameters are model dependent. However, all systems suffer from the same types of defects, more related to forcings, or to defects in model parameterizations that are almost the same for all systems. It is therefore considered that the QC built from GLORYS2V1 may be applied to other systems, assuming that the forecast errors or system biases are of the same magnitude or even lower than those of GLORYS2V1.

4 Scientific assessment results

The MyOcean V2 global system's quality is now assessed in the following and the importance of the scientific validation procedure is demonstrated through the examination of two simulations performed with IRG_DEV and HRZ_DEV systems under development.

4.1 Statistics of observation/best analysis comparisons

The best analyses are first assessed through the examination of direct comparisons with the assimilated observations, and with independent observations that have not been assimilated by the system such as drifting buoys velocity measurements or sea ice observations.

OSD
9, 1123–1185, 2012

4.1.1 Temperature and salinity vertical profiles

The model equivalent at the time and spatial location of the observation is derived from daily averaged analyses (CLASS4 metrics). Statistics (mean and RMS differences) are computed in 2° by 2° bins or in wider (up to basin scale) regions, and in vertical layers.

When the observational dataset has been assimilated, the resulting scores can be considered as residuals of data assimilation. We present here these scores for in situ temperature and salinity vertical profiles which are assimilated in the systems. Part of these data is discarded before the data assimilation takes place, by the means of a first external quality check based on regional departures from climatology. Note that at the validation stage, the original observational dataset is used, and large differences may appear locally. It sometimes points out outliers or erroneous profiles. As can be seen in Fig. 4a, IRG_V1V2 yearly mean departures from observed temperature is not larger than 0.3 °C in many regions of the ocean on average in the first 500 m of the ocean. The largest RMS differences take place in high mesoscale variability regions such as the Gulf Stream, the Kuroshio, the Agulhas current or the Zapiola eddy. The thermoclines of the tropical basins also display significant signatures in the temperature RMS error, especially in the Tropical Pacific where a La Niña event took place throughout most of the year 2010. The salinity average departures from observations stay below 0.03 psu in most regions of the ocean (Fig. 4b). The principal mesoscale activity regions also display higher salinity RMS values. The IRG_DEV system displays similar temperature and salinity RMS difference patterns (not shown). However, some improvements in the Mediterranean region, the Bay of Biscay, the Gulf Stream and the Western Tropical Pacific can be attributed to the use of the adjusted MDT and a more adapted specification of observation errors for SST and SLA. These improvements are highlighted by looking at time series of basin scale statistics. Figures 5 and 6 show temperature and salinity statistics performed in the 5–100 m layer and in the basin scale zones of the North Atlantic, Mediterranean Sea and Indian Ocean. To compare all systems "V1V2" and "DEV", the common period 2007–2011 has been chosen. The HRZ_V1V2 system

OSD
9, 1123–1185, 2012

(dashed line) is only available from October 2009 (see Fig. 1 and Sect. 2.2). Moreover, the results of this system are not representative before 1 January 2010 because a few months of spin up are necessary. So, the time series was complemented by the HRZ_V1 system (solid line).

We initially checked that all the systems were closer to the observations than the climatology. The RMS residuals in temperature and salinity are significantly reduced in the North Atlantic and Mediterranean Sea with IRG_DEV and HRZ_DEV systems. However, IRG_DEV system tends to drift towards a cold and salty subsurface bias in the Indian Ocean. These biases are of the order of magnitude of 0.2 °C and 0.02 psu on basin average between 5 and 100 m. All regions experience these slight biases (not shown) except the North Atlantic, the Mediterranean Sea and the Arctic Ocean. As a consequence, the HRZ_DEV system does not display biases except in the Tropical Atlantic. Finally, no significant improvement is diagnosed in Mediterranean for HRZ_DEV system compared to HRZ_V1V2 system because the latter already benefits from several upgrades (see Sect. 2.2), which can explain that no major improvement is measured in the HRZ_DEV experiment.

4.1.2 Independent SST observations

Yearly mean SST differences with OSTIA observations (not assimilated) show that in the Antarctic, Indian and Atlantic basins the model SST is very close to OSTIA, with difference values staying below the observation error of 0.6 °C (Donlon et al., 2012) on average (Fig. 7). However, strong regional biases are diagnosed in IRG_V1V2 system, particularly for the high northern latitudes and/or some coastal areas. Part of these coastal biases comes from the use of RTG for data assimilation in IRG_V1V2 as this SST product is known to be too cold in the high latitudes coastal regions. These biases disappear in the new version of the system as AVHRR + AMSRE is assimilated. This SST product has the same quality level as OSTIA and both display better performance than RTG especially in high latitudes. Another reason that could explain some of these biases lies in the way the data are assimilated into the system. In IRG_DEV system,

OSD
9, 1123–1185, 2012

the choice has been made not to trust SST and SLA observations within 50 km off the coast and to prescribe higher observation errors in these coastal areas. In IRG_V1V2 system the SST and SLA observation errors do not increase near the coast, which partly generate these large coastal biases diagnosed in the Northern Hemisphere.

The cold bias that persists in the Eastern half of the Pacific in IRG_DEV is not explained by differences between OSTIA and the assimilated AVHRR + AMSRE. This model bias experience peaks over 1 °C and reaches its highest amplitude during summer. If we look at the 2010 average SST increment and its part rejected by the system (Fig. 7e,f), we can see a significant rejection at the place of the cold bias in eastern half of the Pacific. The spatial structure of the bias is also correlated with the very strong La Niña event taking place in 2010 which resulted in cold anomalies over the whole Eastern Pacific. The concurrent effects of bulk fluxes and of IAU correction are not efficient in this region. Fluxes correction methods are under investigation.

4.1.3 Ice observations

The sea ice concentration and drift in the Arctic of IRG_V1V2 analyses are compared with satellite observations in winter (Fig. 8) and in summer (Fig. 9) of the year 2010. The seasonal cycle, the interannual variability and the recent trend of the sea ice extent have already been evaluated and compare well with the satellite estimates (Garric et al., 2008; Lique et al., 2011). The sea ice extent is realistic in all IRG systems. The main spatial patterns of the sea ice drift such as the Beaufort Gyre and the Transpolar Drift Stream are well reproduced by the system. However, the modelled sea ice speed is overestimated whatever the seasons (Figs. 8 and 9) and gives the quickest velocities over the unobserved marginal sea ice-open ocean zones. In summer, the sea ice concentration of IRG_DEV is again more realistic than IRG_V1V2, especially in the Laptev Sea. The HRZ sea ice concentrations and drifts in the North Atlantic are very close to IRG equivalent fields both in summer and winter (not shown), testifying a good performance of the damping of ice condition from IRG to HRZ north open boundaries. The more realistic pattern of sea ice concentration in IRG_DEV system compared to

OSD
9, 1123–1185, 2012

IRG_V1V2 one, over the Laptev Sea and in the Barents Sea, is closely linked with the switch of assimilated SST observation from RTG to AVHRR + AMSRE. Indeed, as it is shown on Fig. 10, comparison of sea-surface temperatures in the two products in the Arctic region shows that AVHRR + AMSRE is substantially warmer, the misfit with RTG reaching more than 5 °C in summer at a few locations off the Siberian coast. Moreover, during wintertime, these warmer SSTs prevent the too important spread of the modelled sea ice towards the open ocean and lead to a very realistic Arctic sea ice envelop. The time evolution of the sea ice extent in the Arctic and in the Antarctic is displayed in Fig. 11. Both IRG_V1V2 and IRG_DEV systems display a seasonal cycle locked in phase with observations. The assimilation of a colder AVHRR + AMSRE SST compared to the RTG SST product allows the IRG_DEV system to keep a wider sea ice extent in the Weddell Sea and a presence of sea ice in the East Antarctica (not shown); this results in a realistic summer Antarctica sea ice. However, these colder SSTs lead to a slight overestimation of the ice extent during wintertime.

4.1.4 Drifter velocities

In order to assess the quality of surface currents, we compare IRG_V1V2 ocean velocity analyses at 15 m with measurements from drifting buoys. Based on recent work published by Grodsky et al. (2011), we compute a downwind slippage correction for drifting buoys velocities of about 0.07 % of the wind speed at 10 m. Then, we apply an algorithm to detect the presence of undrogued drifters in order to add a windage correction (up to 3 %) upon U and V components. This quality control detects about 40 % of the original data set and cleans the high latitude regions (Antarctic Circumpolar Current, North Atlantic drift). Once this correction (that we will refer to as Mercator Océan correction) is applied to the drifter observations, the zonal and meridional velocities of the model at 15 m depth are more consistent with the observations (Fig. 12a).

OSD
9, 1123–1185, 2012

Mean relative velocity bias (MRVB) using all drifters' observations during the year 2010 can be computed as follows:

$$\mathrm{MRVB}(i,j) = \frac{\|\mathrm{velocity}_{\mathrm{drifter}}(i,j)\| - \|\mathrm{velocity}_{\mathrm{model}}(i,j)\|}{\|\mathrm{velocity}_{\mathrm{drifter}}(i,j)\|} \quad (1)$$

where $\mathrm{velocity}_{\mathrm{drifter}}$ is the drifter horizontal velocity, $\mathrm{velocity}_{\mathrm{model}}$ the model horizontal velocity and (i,j) the geographical position of drifter observation.

Figure 12b shows that IRG_V1V2 underestimates the surface velocity from 20 to 50 % in the northern and southern mid and high latitude eastward currents such as the Kuroshio, the North Pacific current, the Gulf Stream, the North Atlantic drift and the Antarctic Circumpolar Current. On the contrary, the tropical westward currents such as the North and South Equatorial currents in the Pacific and in the Atlantic are generally overestimated by 20 to 50 %. The direction errors are much smaller than the velocity amplitude errors, and large direction errors are very local (Fig. 12c). These direction errors generally correspond to ill positioned strong current structures in high mesoscale variability regions (Gulf Stream, Kuroshio, North Brazil Current, Zapiola eddy, Agulhas current, Florida current, East African Coast current, Equatorial Pacific Countercurrent). The IRG_DEV experiment displays similar results (not shown) with a slight improvement in the Western Tropical Pacific, which can be attributed to the adjusted MDT used.

4.2 Statistics of observation/forecast comparisons

4.2.1 Sea level anomaly

Concerning the SLA, the Fig. 13 presents, for IRG_V1V2 and IRG_DEV systems, temporal mean sea level innovation (a and b) and temporal mean sea level residual (c and d) for the year 2010. These two diagnostics illustrate the forecast and analysis scores in a geographical context, highlighting qualities and deficiencies of the system. First, we can suspect in the two versions of IRG system, a likely inconsistency between the MDT and the observed SLA, notably near the Hudson Bay, the Indonesian

OSD
9, 1123–1185, 2012

throughflow, the Caribbeans, and the continental shelves (Island, UK). It may be noted that IRG_DEV innovations within these geographic areas are not reduced by the analysis correction, whereas they are everywhere else (Fig. 13d). This can be attributed to a wider observation error of SLA observation within 50 km off the coast and on the shelves (Fig. 13f), not trusting the data in these areas (same problem with SST). Moreover, higher SLA observation errors have been prescribed in IRG_DEV compared to IRG_V1V2 (Fig. 13e,f) in order to give less weight to SLA observation in the multivariate analysis. The specification of a too low SLA observation error results in unrealistic increments of ill controlled variables, such as salinity and/or horizontal velocities (not shown).

Figure 14 represents temporal series of some HRZ statistics which constitutes forecast scores on the seven days of the assimilation window and allows checking the consistency of the system (Lellouche and Tranchant, 2003). This figure illustrates the evolution of statistics in time but also the performance related to the different changes of versions of the HRZ system. For that, only Jason1 and Jason2 altimeters, present throughout the period 2007–2011, were considered. The forecasting scores of SLA for the different versions of HRZ are globally similar. The biases are weak as the mean innovation is close to zero (Fig. 14c). The RMS of this innovation (Fig. 14a) is of the order of a little less than 8 cm. It is smaller than the different internal errors involved in the system. Moreover, the model is able to explain the observed signal as shown by the ratio RMS misfit over RMS data, which decreases with time and converges towards a value less than 1 (Fig. 14b). In particular, it can be noted a slight improvement to version changes as illustrated by HRZ_V1V2 and HRZ_DEV systems that offer the best RMS misfit at the end of the simulation (of the order of 7 cm).

Murphy Skill Score (MSS) (Murphy, 1988) on the 2007–2011 period, using all available SLA observations inside the assimilation window, have also been computed as follows:

$$\mathrm{MSS} = 1 - \frac{\sum(\mathrm{SLA}_{\mathrm{obs}} - \mathrm{SLA}_{\mathrm{forecast}})^2}{\sum(\mathrm{SLA}_{\mathrm{obs}} - \mathrm{SLA}_{\mathrm{persistence}})^2} \quad (2)$$

OSD
9, 1123–1185, 2012

This score is positive (negative) when the accuracy of the forecast is greater (less) than the accuracy of the persistence. Moreover, MSS = 1 when the forecast is perfect (equal to the observation) and MSS = 0 when the forecast is equivalent to the persistence. Figure 15 shows, for the main GODAE regions, the accuracy of the SLA forecast which can be translated into a measure of percentage improvement in accuracy simply by multiplying the right-hand side of Eq. (2) by 100. The IRG_DEV and HRZ_DEV systems improve the skill scores for all GODAE regions, compared with previous systems, even if some MSS are still negative, particularly in the North Atlantic and Antarctica.

4.2.2 Temperature and salinity vertical profiles

As for the SLA, some diagnostics on the assimilated *T*/*S* vertical profiles have been performed with IRG_V1V2 and IRG_DEV systems. Time series of temperature (Fig. 16) and salinity (Fig. 17) mean residuals in the North Pacific GODAE region reveal a slight drift from the beginning of the year 2009 with IRG_DEV system. The model becomes too cold (0.2 °C in the first 300 m) and too salty (0.05 psu in the first 100 m). Some biases are also observed for free simulation (without data assimilation) and are mainly due to new model parameterizations and atmospheric forcing corrections (see Sect. 2.3). The data assimilation and bias correction stages do not correct this drift but reduce efficiently the errors. Indeed, the RMS of temperature and salinity residuals is reduced for IRG_DEV system for all vertical layers.

We now examine the Pacific region north of 45° N. This region of low salinity (less than 33 psu) gains about 2 mm day^{-1} of freshwater, not mentioning the Amur River flowing in the Okhotsk Sea and the American rivers. We saw that IRG systems suffer from a cold bias in this area (Fig. 7a,b). Figure 18 shows the box averaged innovations of temperature and salinity along time and depth. The top left panel reveals that the cold bias of IRG_V1V2 only concerns the warm season. There is a lack of stratification above 100 m which disappears in the cold season. The stratification is improved in IRG_DEV (top right), even is the surface cold bias remains. IRG_V1V2 has a salty bias in the mixed layer, and a nearly constant fresh bias just below 100 m (bottom left).

OSD
9, 1123–1185, 2012

Both weaknesses are reduced in IRG_DEV (bottom right). Another default present in IRG_V1V2 becomes now more visible. The salinity excess in the warm season is mixed downwards in winter (in blue on the figure). It results in a salty (and cold) bias between 200 m and 300 m, peaking in winter 2010–2011. We checked that the correction of the precipitations lead to a deficit in summer, in a broad region with a maximum near 150° W–35° N, and another along the coasts from Oregon to British Columbia. Another factor is the vertical turbulence closure which neglects the seasonal cycle of wave mixing. It is strongly marked in this region. This contributes to an excess mixing in summer.

4.3 Physical processes

The accuracy of analysis and forecast does not fully demonstrate that the physics of the model are realistic. We have seen that the skill of the models' forecast with respect to the persistence is not significant in many regions. In this section, we measure the improvement of the model skill from one version to the other by studying a range of physical processes and propagations in time.

4.3.1 Water masses

The OVIDE repetitive section in the North Atlantic is sampled every other year since 1997 (Lherminier et al., 2007). The North Atlantic is the place of formation of deep water flowing southward that together with northward surface heat transport via the North Atlantic drift form the Atlantic Meridional Overturning Cell. Moreover, this section samples the Mediterranean outflow in the Atlantic near 1000 m which is an important feature of the circulation and water masses characteristics in the North East Atlantic near European coasts. A good representation of the North East Atlantic water masses is crucial for the nesting of MyOcean regional systems such as Iberian-Biscay-Ireland system (Maraldi et al., this issue 2012) and North-West-Shelves system (O'Dea et al., 2010). It is not surprising that IRG and HRZ systems both compare well with temperature (not

OSD
9, 1123–1185, 2012

shown) and salinity (Fig. 19) measurements along the OVIDE section in 2010 as those observations are assimilated. However, the HRZ_DEV analyses of surface salinity in the vicinity of 11.5° W are closer to OVIDE measurements than any other analyses. The Mediterranean outflow is better represented, especially in salinity. The better salinity accuracy of HRZ_DEV with respect to HRZ_V1V2 can be partly explained by an earlier initialization of the system (in October 2006 for HRZ_DEV instead of October 2009 for HRZ_V1V2), and consequently, a bias correction algorithm working at its full capacity. To that should be added the high quality of AVHRR + AMSRE SST product and consequently corrections of salinity resulting from the multivariate analysis. Thus, this hydrological section (CLASS2 metric) shows the interest of using the HRZ system as a refinement of the global solution in the North Atlantic and Mediterranean.

4.3.2 Tropical waves

The realism of tropical oceans is crucial for seasonal forecasting applications. The most significant ocean/atmosphere coupling signals are found in the tropical band such as El Niño Southern Oscillation (ENSO) which atmospheric teleconnexions are global. The Indian Ocean also plays a role in the modulation of ENSO and of the Asian Monsoon and the Tropical Atlantic is linked with African Monsoons (Redelsperger et al., 2006). As the realism of the heat content is ensured through the examination of observation minus model differences in Sect. 4.1, it is necessary to check that important physical processes taking place in the tropics such as Kelvin, Rossby and Tropical instability waves are well reproduced. Westward Rossby and eastward Kelvin waves propagations (Delcroix et al., 1991) appear in longitude-time Hovmöller diagrams of SLA at the equator, as can be seen in Fig. 20. The waves amplitude as well as their propagation speed are realistic in IRG_V1V2 system with respect to the merged SLA observations. Consistent with Delcroix et al (1991), the Kelvin waves cross the Pacific Ocean in approximately 2 to 3 months (their phase speed is O(3 m s^{-1})) and their amplitude is O(15 cm) or more. Rossby waves are three times slower (9 months to cross the Pacific, speed is O(1 m s^{-1})) and their amplitude is weaker (O(10 cm)). No difference is

OSD
9, 1123–1185, 2012

observed between IRG_V1V2 and IRG_DEV in this case (not shown). The systems stay close to the observations without inducing shocks or physical inconsistencies thanks to the IAU correction and the model is allowed to produce smooth propagations. This was an important improvement with respect to previous sequential systems where important data assimilation jumps could be diagnosed (not shown).

The tropical instability waves (TIW) can be diagnosed in SST (Chelton et al., 2000). These waves initiate at the interface between areas of warm and cold sea surface temperatures near the Equator and form a regular pattern of westward-propagating waves. Longitude time diagrams at the latitude 3° N show TIW mainly in the Pacific and Atlantic Oceans in the eastern parts of the basins (Fig. 21). Comparable TIW appear in IRG_V1V2 system but their amplitude is slightly underestimated with respect to AVHRR + AMSRE as can be seen in Fig. 21. The IRG_DEV system assimilates AVHRR + AMSRE SST product. In consequence, IRG_DEV is even locally closer to this particular SST product than IRG_V1V2 which assimilates RTG (not shown). Again, errors (or benefits) of the input data are transferred to the monitoring and forecasting systems. The HRZ_DEV system, as HRZ_V1V2 one, displays TIW that are of slightly higher amplitude than IRG systems' TIW in the Tropical Atlantic (not shown).

4.3.3 Equatorial under current

We looked more closely at another physical process which is the equatorial pacific current system. We can see in Fig. 22 that the IRG_V1V2 EUC (Equatorial Under Current) does not penetrate west of 165° E and deeper than 100 m. This problem generates an upwelling in this area and changes the water mass properties and transport in the Indonesian throughflow. The poor representation of the EUC generates errors in the Pacific and Indian Oceans. MDT and its associated error have been adjusted in the IRG_DEV experiment by combining the MDT used by IRG_V1V2 experiment and GOCE (Gravity field and steady-state Ocean Circulation Explorer) data. An important consequence of this change is that the EUC is continuous over the whole equatorial Pacific in IRG_DEV experiment, as observed by Johnson et al. (2005) and Marin et al. (2010).

OSD
9, 1123–1185, 2012

ADCP observations, from the TAO array of moorings (http://www.pmel.noaa.gov), confirm the improvement of subsurface velocities near 165° E at the Equator. The EUC is well marked in the observations from 2007 to 2011, and its amplitude of about 1 m s^{-1} is well represented by IRG_DEV while it is underestimated by IRG_V1V2.

4.4 Stability in time, trends and biases

Regional biases with respect to assimilated and independent data have been identified below, and a set of important physical processes have been validated for the year 2010. It is now important to verify the long term behavior of the system over the whole 2007–2011 period. The global cumulative trends of temperature at 300 m are displayed in Fig. 23. There is a noticeable cooling East of the Philippines, and two regions of warming West of Australia in IRG_V1V2 (Fig. 23a). These signals are also present in IRG_DEV (Fig. 23b) but cooling is generally reinforced. The North and South Atlantic are regions of clear cooling in IRG_DEV. When compared to the IRG_DEV temperature innovations near 300 m (Fig. 24), the cumulative trend exceeds the bias in the above mentioned regions. In the North East Pacific, the cooling trend is comparable to the innovations. There are other regions where the trend from IRG_DEV is not reliable (South Pacific East of Australia, South Indian between Madagascar and Australia...).

The variability of the system's behaviour (variability of increments) can be assessed with an Empirical Orthogonal Function (EOF) analysis. The first EOF of surface temperature increment (Fig. 25) gives the major spatial directions of the surface temperature correction. The associated time series (principal component) shows the evolution in time of this dominant correction pattern. The latter confirms the seasonality of the cold bias that is observed, in particular in the North Pacific. The amplitude of this bias is reduced in IRG_DEV experiment. The other dominant directions of correction (all variables) are very similar in IRG_V1V2 and IRG_DEV (not shown). These results suggest that the data assimilation system is not responsible for the general cold trend appearing in IRG_DEV. This confirms the hypothesis of (external) flux correction problems.

OSD
9, 1123–1185, 2012

To conclude, we have identified drifts that can be, and must be corrected if one want use these systems for climate studies. This "stability" metric prevents us from releasing IRG_DEV and HRZ_DEV systems.

5 Conclusions

The Mercator Ocean global monitoring and forecasting system (MyOcean V2 global MFC) is evaluated for the period 2007–2011 with a thorough procedure involving statistics of departures from observations and physical processes assessment. The accuracy of the V2 system (including the global 1/4° IRG_V1V2 and its 1/12° North Atlantic and Mediterranean zoom HRZ_V1V2) is clearly better than the climatology. Performances are stable in time and should be reliable on the long term.

All monitoring systems are close to SLA observations with forecast (range 1 to 7 days) RMS difference of 7 cm. It is smaller than the intrinsic variability of the SLA observations. The dominant source of error in sea level comes from the uncertainty in MDT. The global IRG gives an accurate description of water masses almost everywhere between the bottom and 500 m. Between 0 and 500 m, departures from in situ observations rarely exceed 1 °C and 0.2 psu. Exceptions concern some high variability regions like the Gulf Stream or the Eastern Tropical Pacific. Most departures from SST observations do not exceed the intrinsic error of the observations O(0.6 °C).

During the summer season, the systems stratification is a little weak. Excess mixing results in cold biases near the surface and warm biases in subsurface. This bias is particularly marked in IRG_DEV. A large scale bias of more than 1 °C appears in boreal summer in the North Pacific gyre. This regional bias takes place in a region where the mixed layer is already thin. The bias could be attributed to the atmospheric forcing and/or the bio-optic properties of the seawater. The system is not efficient enough in correcting the SST because heat fluxes are not part of the estimated state. We checked that most of the SST correction is swept away by the bulk forcing function.

OSD
9, 1123–1185, 2012

A windage and slippage correction developed by Mercator Océan is applied to cope with the drogue loss of the surface drifter. The surface currents are underestimated in the mid-latitudes and overestimated at the equator with respect to the corrected drifter velocities. The underestimation ranges from 20 % in strong currents up to 60 % in weak currents. The orientation of the current vectors is well represented.

Despite the IRG systems does not include any assimilation of sea ice quantities, they reproduce the sea ice seasonal lifecycle in a very realistic manner. Thanks to the assimilation of the AVHRR + AMSRE SST product, the IRG_DEV system represent significantly better the frontier between sea ice and the open ocean, especially during summer time.

The same scientific assessment procedure was conducted on IRG_DEV and HRZ_DEV. Diagnostics were compared with the MyOcean version IRG_V1V2 and HRZ_V1V2. Improvements are the rule. The update of the MDT (and its error) corrects local biases in the Indonesian throughflow and in the Western Tropical Pacific. This improves the subsurface currents at the Equator.

Earlier studies have shown that RTG SST data suffer from a cold bias near the coasts. The validation team has proposed to use AVHRR + AMSRE product instead. Statistics show that this dataset helps to significantly reduce the surface temperature and salinity biases, as well as RMS differences. The sea ice concentration in both Arctic and Antarctica also benefit from the assimilation of a SST product of better quality.

The scientific quality assessment procedure has detected a drift of the performance of IRG_DEV system in 2009, two years after the start. A cold and salty slight bias is developing near 100 m. HRZ_DEV system is less marked and it concerns only water deeper than 2000 m. The drift is a combined effect of the new model parameterizations and forcings. The use of a new SST dataset may have an impact. This data assimilation does not correct the air/sea fluxes. The IAU prevent from keeping the correction of the initial condition in the model because of the bulk formulation.

IRG_DEV and HRZ_DEV systems have better statistics in spite of this drift. But this drift prevent from putting the upgrade in real time. It demonstrates that several years

OSD
9, 1123–1185, 2012

have to be performed and thoroughly assessed before transitioning to a new version, especially if new model parameterizations are involved.

Several scientific and technical choices are validated here such as the use of AVHRR + AMSRE SST for data assimilation, the use of a MDT adjusted with GOCE and with the systems innovations, and the parameterization of observation and representativity error covariances. We will use IRG and HRZ systems to test new parameterizations for the future global high resolution 1/12° system (HRG) due to its cost limitation. The current free model configuration of the future HRG system does not exhibit the drifts diagnosed in IRG_DEV. The next version of HRG will include the above validated changes. A correction of the air temperature will also be introduced in order to avoid the damping of increments via the bulk forcing function.

Acknowledgements. This work is supported by the MyOcean FP7 project. Special thanks to our Mercator Océan and CLS colleagues, and to our collaborators of the DRAKKAR project and NEMO group, CORIOLIS, AVISO, and GMMC scientists.

References

Antonov, J. I., Locarnini, R. A., Boyer, T. P., Mishonov, A. V., and Garcia, H. E.: World Ocean Atlas 2005, Vol. 2: Salinity, in: NOAA Atlas NESDIS 62, edited by: Levitus, S., US Government Printing Office, Washington, DC, 182 pp., 2006.

Arakawa, A. and Lamb, V. R.: A potential enstrophy and energy conserving scheme for the shallow water equations, Mon. Weather. Rev., 109, 18–36, 1981.

Barnier, B., Madec, G., Penduff, T., Molines, J. M., Treguier, A. M., Le Sommer, J., Beckmann, A., Biastoch, A., Böning, C., Dengg, J., Derval, C., Durand, E., Gulev, S., Remy, E., Talandier, C., Theetten, S., Maltrud, M., McClean, J., and De Cuevas, B.: Impact of partial steps and momentum advection schemes in a global circulation model at eddy permitting resolution, Ocean Dynam., 56, 543–567, 2006.

Benkiran, M. and Greiner, E.: Impact of the incremental analysis updates on a real-time system of the North Atlantic Ocean, J. Atmos. Ocean. Tech., 25, 2055–2073, 2008.

OSD

9, 1123–1185, 2012

Blanke, B. and Delecluse, P.: Variability of the Tropical Atlantic-Ocean simulated by a general-circulation model with 2 different mixed-layer physics, J. Phys. Oceanogr., 23, 363–1388, 1993.
Bloom, S. C., Takas, L. L., Da Silva, A. M., and Ledvina, D.: Data assimilation using incremental analysis updates, Mon. Weather Rev., 124, 1256–1271, 1996.
Bernie, D. J., Woolnough, S. J., Slingo, J. M., and Guilyardi, E.: Modeling diurnal and intraseasonal variability of the ocean mixed layer, J. Climate, 18, 1190–1202, 2005.
Cabanes, C., Grouazel, A., Von Schuckmann, K., Hamon, M., Turpin, V., Coatanoan, C., Guinehut, S., Boone, C., Ferry, N., Reverdin, G., Pouliquen, S., and Le Traon, P. Y.: The CORA dataset: Validation and Diagnostics of ocean temperature and salinity in situ measurement, Ocean Sci., submitted, 2012.
Chelton, D. B., Wentz, F. J., Gentemann, C. L., De Szoeke, R. A., and Schlax, M. G.: Satellite microwave SST observations of transequatorial tropical instability waves, Geophys. Res. Lett., 27, 1239–1242, 2000.
Chen, J. L., Wilson, C. R., Tapley, B. D., Famiglietti, J. S., and Rodell, M.: Seasonal global mean sea level change from satellite altimeter, GRACE, and geophysical models, J. Geodesy, 79, 532–539, doi:10.1007/s00190-005-0005-9, 2005.
Cravatte, S., Madec, G., Izumo, T., Menkes, C., and Bozec, A.: Progress in the 3-D circulation of the Eastern Equatorial Pacific in a climate, Ocean Model., 17, 28–48, 2007.
Crosnier, L. and Le Provost, C.: Inter-comparing five forecast operational systems in the North Atlantic and Mediterranean basins: the MERSEA-strand1 methodology, J. Marine Syst., 65, 354–375, 2007.
Cummings, J., Bertino, L., Brasseur, P., Fukumori, I., Kamachi, M., Martin, M. J., Mogensen, K., Oke, P., Testut, C. E., Verron, J., and Weaver, A.: Ocean data assimilation systems for GODAE, Oceanography, 22, 6–109, 2009.
Dai, A. and Trenberth, K. E.: Estimates of freshwater discharge from continents: latitudinal and seasonal variations, J. Hydrometeorol., 3, 660–687, 2002.
Delcroix, T., Picaut, J., and Eldin, G.: Equatorial Kelvin and Rossby waves evidenced in the Pacific Ocean through Geosat Sea Level and Surface Current Anomalies, J. Geophys. Res., 96, 3249–3262, 1991.
Donlon, C. J., Martin, M., Stark, J. D., Roberts-Jones, J., Fiedler, E., and Wimmer, W.: The Operational Sea Surface Temperature and Sea Ice Analysis (OSTIA) system, Remote Sens. Environ., 116, 140–158, 2012.

OSD
9, 1123–1185, 2012

Elmoussaoui, A., Perruche, C., Greiner, E., Ethé, C., and Gehlen, M.: Integration of biogeochemistry into Mercaor Océan systems, Mercator Océan Newsletter 40: MyOcean Ecosystem Models, 3–14, 2011.
Ezraty, R., Girard-Ardhuin, F., Piolle, J. F., Kaleschke, L., and Heygster, G.: Arctic and Antarctic sea ice concentration and Arctic sea ice drift estimated from Special Sensor Microwave data, User's Manuel Version 2.1, CERSAT, 2007.
Ferry, N., Parent, L., Garric, G., Drévillon, M., Desportes, C., Bricaud, C., and Hernandez, F.: Scientific Validation Report (ScVR) for V1 Reprocessed Analysis and Reanalysis (MYO-WP4-ScCV-rea-MERCATOR), MyOcean report, 66 pp., 2011.
Fichefet, T. and Maqueda, M. A.: Sensitivity of a global sea ice model to the treatment of ice thermodynamics and dynamics, J. Geophys. Res., 102, 12609–12646, 1997.
Garric, G., Verbrugge, N., Bouillon, S., and Vancoppenolle, M.: Preliminary assessment of sea ice in the global 1/4° Mercator Ocean forecasting system, Mercator Océan Newsletter 28, 2008.
Garric, G., Verbrugge, N., and Bricaud, C.: Large scale ERAinterim radiative and precipitation surface fluxes assessment, correction and application on 1/4° global ocean 1989–2009 hindcasts, EGU General Assembly 2011, Vienna, Austria, 2011.
Gemmill, W., Bert, K., and Xu, L.: Daily Real-Time Global Sea Surface Temperature – High Resolution Analysis at NOAA/NCEP, NOAA/NWS/NCEP/MMAB Office Note Nr. 260, 39 pp., 2007.
Goosse, H., Campin, J. M., Deleersnijder, E., Fichefet, T., Mathieu, P. P., Maqueda, M. A. M., and Tartinville, B.: Description of the CLIO model version 3.0, Institut d'Astronomie et de Geophysique Georges Lemaitre, Catholic University of Louvain (Belgium), 2001.
Grodsky, S. A., Lumpkin, R., and Carton, J. A.: Spurious trends in global surface drifter currents, Geophys. Res. Lett., 38, L10606, doi:10.1029/2011GL047393, 2011.
Hernandez, F., Bertino, L., Brassington, G. B., Chassignet, E. P., Cummings, J., Davidson, F., Drévillon, M., Garric, G., Kamachi, M., Lellouche, J. M., Mahdon, R., Martin, M. J., Ratsimandresey, A., and Régnier, C.: Validation and intercomparison studies within GODAE, Oceanography, 22, 128–143, 2009.
Huang, X. Y., Mogensen, K. S., and Yang, X.: First-guess at appropriate time: the HIRLAM implementation and experiments, Proc. HIRLAM Workshop on Variational Data Assimilation and Remote Sensing, Helsinki, Finland, Finnish Meteorological Institute, 28–43, 2002.

OSD
9, 1123–1185, 2012

Hunke, E. C. and Dukowicz, J. K.: An elastic-viscous-plastic model for sea ice dynamics, J. Phys. Oceanogr., 27, 1849–1867, 1997.
Jacobs, S., Hellmer, H., Doake, C. S. M., Jenkins, A., and Frolich, R. M.: Melting of ice shelves and the mass balance of Antarctica, J. Glaciol., 38, 375–387, 1992.
Johnson, G. C., Sloyan, B. M., Kessler, W. S., and McTaggart, K. E.: Direct measurements of upper ocean currents and water properties across the Tropical Pacific Ocean during the 1990's, Prog. Oceanogr., 52, 31–61, doi:10.1016/S0079-6611(02)00021-6, 2002.
Koch-Larrouy, A., Madec, G., Blanke, B., and Molcard, R.: Water mass transformation along the Indonesian throughflow in an OGCM, Ocean Dynam., 58, 289–309, doi:10.1007/s10236-008-0155-4, 2008.
Large, W. G. and Yeager, S. G.: The global climatology of an interannually varying air–sea flux data set, Cim. Dynam., 33, 341–364, doi:10.1007/s00382-008-0441-3, 2009.
Lellouche, J. M. and Tranchant, B.: Les diagnostics d'assimilation dans PSY2, Mercator Océan Newsletter 9, 25 pp., 2003.
Lévy, M., Estublier, A., and Madec, G.: Choice of an advection scheme for biogeochemical models, Geophys. Res. Lett., 28, 3725–3728, doi:10.1029/2001GL012947, 2001.
Lherminier, P., Mercier, H., Gourcuff, C., Alvarez, M., Bacon, S., and Kermabon, C.: Transports across the 2002 Greenland–Portugal OVIDE section and comparison with 1997, J. Geophys. Res., 112, C07003, doi:10.1029/2006JC003716, 2007.
Lique, C., Garric, G., Treguier, A. M., Barnier, B., Ferry, N., Testut, C.-E., and Girard-Ardhuin, F.: Evolution of the Arctic Ocean salinity, 2007–2008: contrast between the Canadian and the Eurasian basins, J. Climate, 24, 1705–1717, 2011.
Locarnini, R. A., Mishonov, A. V., Antonov, J. I., Boyer, T. P., and Garcia, H. E.: World Ocean Atlas 2005, Volume 1: Temperature, in: NOAA Atlas NESDIS 61, edited by: Levitus, S., US Government Printing Office, Washington, DC, 182 pp., 2006.
Lombard, A., Garric, G., and Penduff, T.: Regional patterns of observed sea level change: insights from a 1/4° global ocean/sea-ice hindcast, Ocean Dynam., 59, 433–449, 2009.
Madec, G.: NEMO ocean engine, Note du Pole de modélisation, Institut Pierre-Simon Laplace (IPSL), France, No. 27 ISSN No. 1288–1619, 2008.
Maraldi, C., Chanut, J., Levier, B., Reffray, G., Ayoub, N., De Mey, P., Lyard, F., Cailleau, S., Drévillon, M., Fanjul, E. A., Sotillo, M. G., Marsaleix, P., and the Mercator team: NEMO on the shelf: assessment of the Iberia-Biscay-Ireland configuration, Ocean Sci., submitted, 2012.

OSD
9, 1123–1185, 2012

Marin, F., Kestenare, E., Delcroix, T., Durand, F., Cravatte, S., Eldin, G., and Bourdallé-Badie, R.: Annual reversal of the equatorial intermediate current in the Pacific: observations and model diagnostics, J. Phys. Oceanogr., 40, 915–933, 2010.

Murphy, A. H.: Skill scores based on the mean square error and their relationships to the correlation, coefficient, Mon. Weather Rev., 116, 2417–2424, 1988.

O'Dea, E. J., While, J., Furner, R., Hyder, P., Arnold, A., Storkey, D., John, R. Siddorn, J. R., Martin, M., Liu, H., and Holt, J. T.: NEMO-Shelf, towards operational oceanography with SST data assimilation on the North West European Shelf, Mercator Océan Newsletter 39, 25–28, 2010.

Oke, P. R., Brassington, G. B., Griffin, D. A., and Schiller, A.: The Bluelink Ocean Data Assimilation System (BODAS), Ocean Model., 21, 46–70, 2008.

Ollivier, A. and Faugere, Y.: Envisat RA-2/MWR ocean data validation and cross-calibration Activities, Yearly report, Technical Note CLS.DOS/NT/10.018, Contract N SALP-RP-MA EA-21920-CLS, 2010.

Penduff, T., Le Sommer, J., Barnier, B., Treguier, A.-M., Molines, J.-M., and Madec, G.: Influence of numerical schemes on current-topography interactions in 1/4° global ocean simulations, Ocean Sci., 3, 509–524, doi:10.5194/os-3-509-2007, 2007.

Penduff, T., Juza, M., Brodeau, L., Smith, G. C., Barnier, B., Molines, J.-M., Treguier, A.-M., and Madec, G.: Impact of global ocean model resolution on sea-level variability with emphasis on interannual time scales, Ocean Sci., 6, 269–284, doi:10.5194/os-6-269-2010, 2010.

Pham, D. T., Verron, J., and Roubaud, M. C.: A singular evolutive extended Kalman filter for data assimilation in oceanography, J. Marine Syst., 16, 323–340, 1998.

Redelsperger, J. L., Thorncroft, C., Diedhiou, A., Lebel, T., Parker, D. J., and Polcher, J.: African Monsoon Multidisciplinary Analysis (AMMA): an international research project and field campaign, B. Am. Meteorol. Soc., 87, 1739–1746, 2006.

Reynolds, R. W., Smith, T. M., Liu, C., Chelton, D. B., Casey, K. S., and Schlax, M. G.: Daily high-resolution blended analyses for sea surface temperature, J. Climate, 20, 5473–5496, 2007.

Rio, M. H., Guinehut, S., and Larnicol, G.: New CNES-CLS09 global mean dynamic topography computed from the combination of GRACE data, altimetry, and in situ measurements, J. Geophys. Res., 116, C07018, doi:10.1029/2010JC006505, 2011.

OSD
9, 1123–1185, 2012

Roquet, F., Charrassin, J. B., Marchand, S., Boehme, L., Fedak, M., Reverdin, G., and Guinet, C.: Delayed-mode calibration of hydrographic data obtained from animal-borne satellite relay data loggers, J. Atmos. Ocean. Tech., 28, 787–801, 2011.

Roullet, G. and Madec, G.: Salt conservation, free surface, and varying levels: a new formulation for ocean general circulation models, J. Geophys. Res., 105, 23927–23942, 2000.

Silva, T. A. M., Bigg, G. R., and Nicholls, K. W.: Contribution of giant icebergs to the Southern Ocean freshwater flux, J. Geophys. Res., 111, C03004, doi:10.1029/2004JC002843, 2006.

Talagrand, O.: A posteriori evaluation and verification of analysis and assimilation algorithms, Proc. of ECMWF Workshop on Diagnosis of Data Assimilation System (Reading), 17–28, 1998.

Tranchant, B., Testut, C. E., Renault, L., Ferry, N., Birol, F. and Brasseur, P.: Expected impact of the future SMOS and Aquarius Ocean surface salinity missions in the Mercator Océan operational systems: new perspectives to monitor ocean circulation, Remote Sens. Environ., 112, 1476–1487, 2008.

OSD

9, 1123–1185, 2012

Table 1. Specificities of the Mercator Océan IRG systems. In bold, the major upgrades with respect to previous version.

System acronym	Domain	Resolution	Model	Assimilation	Assimilated observations	MyOcean version	Mercator Océan system reference
IRG_V0	global	Horizontal: 1/4°	ORCA025 NEMO 1.09	SAM (SEEK)	"RTG" SST	V0	PSY3V2R1
		Vertical: 50 levels	LIM2, Bulk CLIO		SLA		
			24 h atmospheric forcing		*T*/*S* vertical profiles		
IRG_V1V2	global	Horizontal: 1/12°	ORCA025 **NEMO 3.1**	SAM (SEEK)	"RTG" SST	V1/V2	PSY3V3R1
		Vertical: 50 levels	**LIM2 EVP, Bulk CORE**	**IAU**	SLA		
			3 h atmospheric forcing	**3D-Var bias correction**	*T*/*S* vertical profiles		
IRG_DEV	global	Horizontal: 1/4°	ORCA025 NEMO 3.1	SAM (SEEK)	**"AVHRR + AMSRE" SST**		PSY3V3R2
		Vertical: 50 levels	LIM2 EVP, Bulk CORE	IAU	SLA		
			3 h atmospheric forcing	3D-Var bias correction	*T*/*S* vertical profiles		
			New parameterization of vertical mixing	**Obs. errors higher near the coast (for SST and SLA) and on shelves (for SLA)**	**MDT "CNES-CLS09" adjusted**		
			Taking into account ocean colour for depth of light extinction		**Sea Mammals *T*/*S* vertical profiles**		
				MDT error adjusted			
			Large scale correction to the downward radiative and precipitation fluxes	**Increase of Envisat altimeter error**			
				QC on *T*/*S* profiles			
			Adding runoff for iceberg melting	**New correlation radii**			
			Adding seasonal cycle for surface mass budget				

OSD
9, 1123–1185, 2012

Table 2. Specificities of the Mercator Océan HRZ systems. In bold, the major upgrades with respect to previous version.

System acronym	Domain	Resolution	Model	Assimilation	Assimilated observations	Inter dependencies	MyOcean version	Mercator Océan system reference
HRZ_V0	Tropical	Horizontal: 1/12°	NATL12 NEMO 1.09	SAM (SEEK)	"RTG" SST		V0	PSY2V3R1
	North Atlantic	Vertical: 50 levels	LIM2, Bulk CLIO		SLA			
	Mediterranean		24 h atmospheric forcing		*T*/*S* vertical profiles			
HRZ_V1	Tropical	Horizontal: 1/12°	NATL12 **NEMO 3.1**	SAM (SEEK)	RTG-SST	**OBC from IRG_V1V2**	V1	PSY2V4R1
	North Atlantic	Vertical: 50 levels	**LIM2 EVP, Bulk CORE**	**IAU**	SLA			
	Mediterranean		**3 h atmospheric forcing**	**3D-Var bias correction**	*T*/*S* vertical profiles			
HRZ_V1V2	Tropical	Horizontal: 1/12°	NATL12 NEMO 3.1	SAM (SEEK)	"AVHRR + AMSRE" SST	OBC from IRG_V1V2	V1/V2	PSY2V4R2
	North Atlantic	Vertical: 50 levels	LIM2 EVP, Bulk CORE	IAU	SLA			
	Mediterranean		3 h atmospheric forcing	3D-Var bias correction	*T*/*S* vertical profiles			
				Obs. errors higher near the coast (for SST and SLA) and on shelves (for SLA)	**MDT CNES-CLS09 adjusted**			
				MDT error adjusted				
				New correlation radii				
HRZ_DEV	Tropical	Horizontal: 1/12°	NATL12 NEMO 3.1	SAM (SEEK)	"AVHRR + AMSRE" SST	OBC from IRG_DEV		PSY2V4R3
	North Atlantic	Vertical: 50 levels	LIM2 EVP, Bulk CORE	IAU	SLA			
	Mediterranean		3 h atmospheric forcing	3D-Var bias correction	*T*/*S* vertical profiles	**Spatial mean evaporation minus precipitation from IRG_DEV**		
			New parameterization of vertical mixing	Obs. errors higher near the coast (for SST and SLA) and on shelves (for SLA)	MDT CNES-CLS09 adjusted			
			Taking into account ocean colour for depth of light extinction		**Sea Mammals *T*/*S* profiles**			
				MDT error adjusted				
			Large scale correction to the downward radiative and precipitation fluxes	New correlation radii				
				Increase of Envisat altimeter error				
				QC on *T*/*S* profiles				

OSD
9, 1123–1185, 2012

Table 3. Types of metrics used for Calibration/Validation during MyOcean.

MERSEA/GODAE classification	Variable	Region	Type of metric	Reference observational dataset
CLASS1	Monthly T and S (3-D)	Global	Visual inspection of seasonal and interannual signal	Levitus 2005 monthly climatology of T/S
	Sea ice concentration and drift	Antarctic and Arctic	Visual inspection of seasonal and interannual signal	CERSAT Sea ice concentration and drift
	SLA and SST	Tropical basins	Visual inspection of Hovmöller diagrams comparisons with satellite observations	AVISO and OSTIA
CLASS2	T, S, U, V, SSH atmospheric forcings	Global at CLASS2 locations	Visual inspection of high frequencies comparisons with observed time series	MyOcean: CORIOLIS
CLASS3	Sea ice concentration	Antarctic and Arctic	Time evolution of sea ice extent	NSIDC sea ice extent from SSM/I observations
	U and V (3-D)	Global	Visual inspection of volume transports through sections	Literature
Data Assimilation statistics	SLA	Global and regional basins	Error = observation minus model Time evolution of RMS and mean error	MyOcean: On track AVISO SLA observations
	SST	Global and regional basins	Error = observation minus model Time evolution of RMS and mean error	"RTG" SST("AVHRR + AMSRE" SST for HRZ)
CLASS4 and Data Assimilation statistics	T and S (3-D)	Global and regional basins	Error = model minus observation Time evolution of RMS error on 0–500 m Vertical profile of mean error.	MyOcean:CORIOLIS $T(z)$ and $S(z)$ profiles
CLASS4	SSH	At tide gauges (Global but near coastal regions)	Error = model minus observation Time series correlation and RMS error	GLOSS, BODC, Imedea, WOCE, OPPE, SONEL
	Surface current U	Global and regional basins	Error = model minus observation Mean error and vector correlation	SVP drifting buoys from CORIOLIS
	Surface current V	Global and regional basins	Error = model minus observation Mean error and vector correlation	SVP drifting buoys from CORIOLIS
	Sea ice concentration	Antarctic and Arctic	Error = observation minus model Time evolution of RMS and mean error	CERSAT Sea ice concentration

OSD
9, 1123–1185, 2012

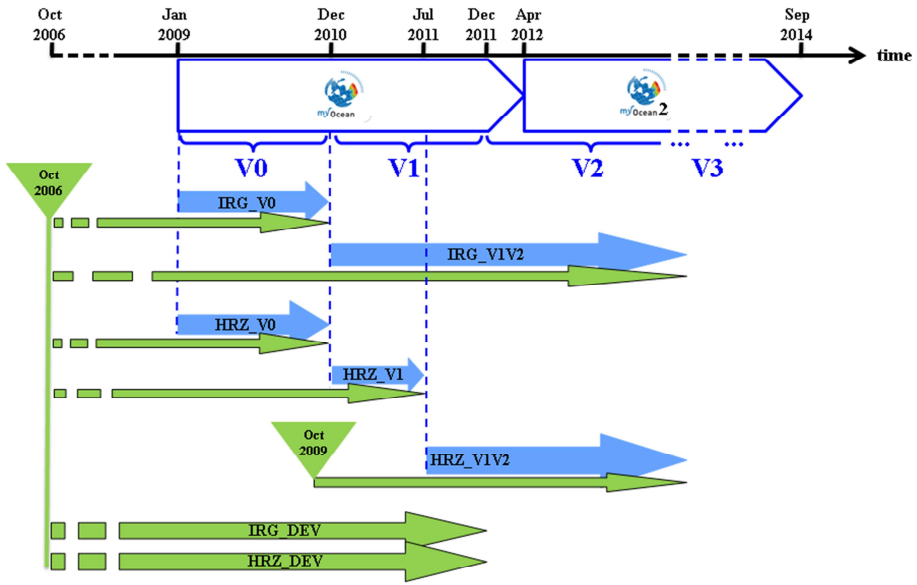

Fig. 1. Timeline of the MyOcean global analysis and forecasting system for the various milestones V0, V1 and V2. Real-time MyOcean production is in blue. Available Mercator Océan simulation is in green including the catch-up to real-time. The latest most advanced versions of systems in terms of scientific developments are named IRG_DEV and HRZ_DEV for intermediate resolution global and high resolution zoom systems respectively.

OSD
9, 1123–1185, 2012

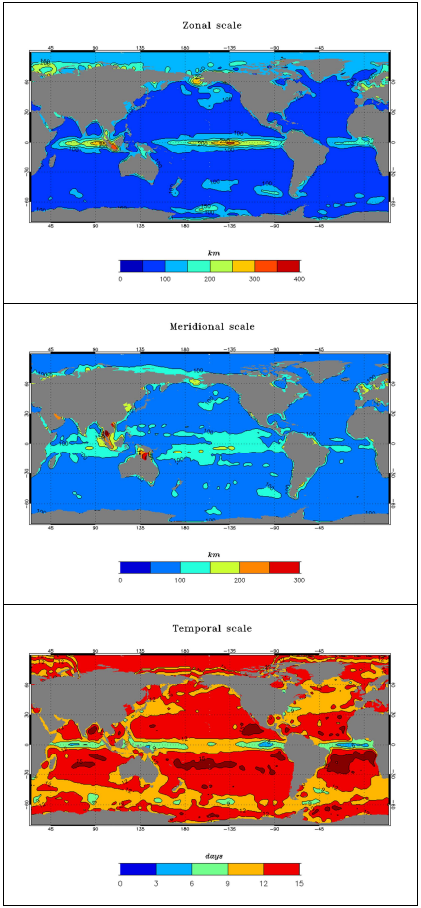

Fig. 2. Zonal, meridional (km) and temporal (days) correlations scales (from top to bottom) used by IRG_DEV, HRZ_V1V2 and HRZ_DEV systems.

OSD
9, 1123–1185, 2012

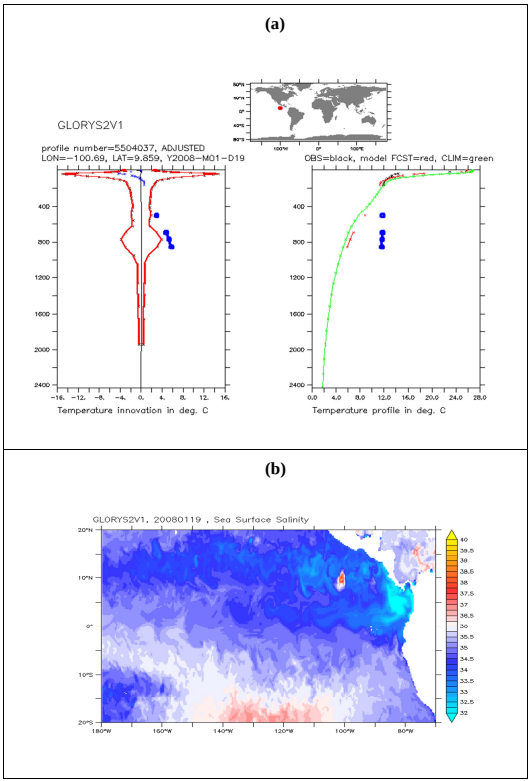

Fig. 3. Example of a suspicious temperature vertical profile at 100.69° W–9.86° N, highlighted by the QC on the CORA3.1 dataset. **(a)** left panel represents temperature innovation profile in blue and temperature innovation threshold in red. Right panel represents the absolute vertical temperature profile (observation in black, climatology in green and model in red). Large blue dots correspond to "bad" innovations or "bad" observations. **(b)** when this profile is assimilated, an abnormal value of salinity appears at the temporal and geographical positions of this profile.

OSD
9, 1123–1185, 2012

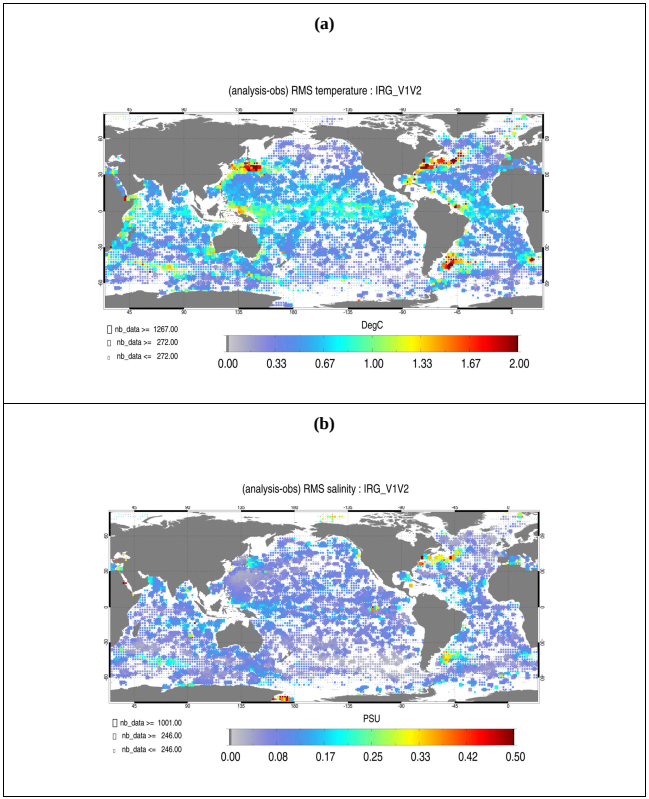

Fig. 4. 2010 temperature **(a)** and salinity **(b)** RMS of the differences between all available observations from the CORIOLIS database and daily mean best analyses for IRG_V1V2 system. Averages are performed in the 0–500 m layer. The size of the pixel is proportional to the number of observations used to compute the RMS in 2° × 2° boxes. Observations that differ by more than 8 °C or 1 psu of a climatological reference do not come into account in the calculation of the diagnostic.

OSD
9, 1123–1185, 2012

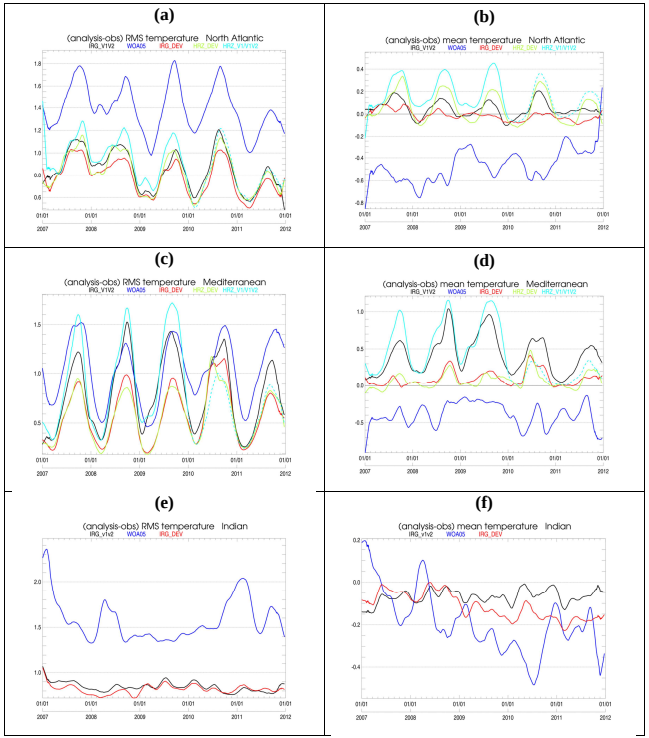

Fig. 5. Temperature (°C) RMS (**a**, **c** and **e**) and mean (**b**, **d** and **f**) differences (best analysis minus observation). For these diagnostics, all available *T*/*S* observations from the CORIOLIS database and Mercator Océan daily average analyses co-localised at the temporal and spatial location of the observations are used. Statistics are displayed for IRG_V1V2 (black line), IRG_DEV (red line), HRZ_V1 (cyan solid line), HRZ_V1V2 (cyan dashed line), HRZ_DEV (green line) and World Ocean Atlas climatology WOA05 (blue line). Averages are performed in the 5–100 m layer in the basin scale zones of the North Atlantic (**a** and **b**), Mediterranean Sea (**c** and **d**) and Indian Ocean (**e** and **f**).

OSD
9, 1123–1185, 2012

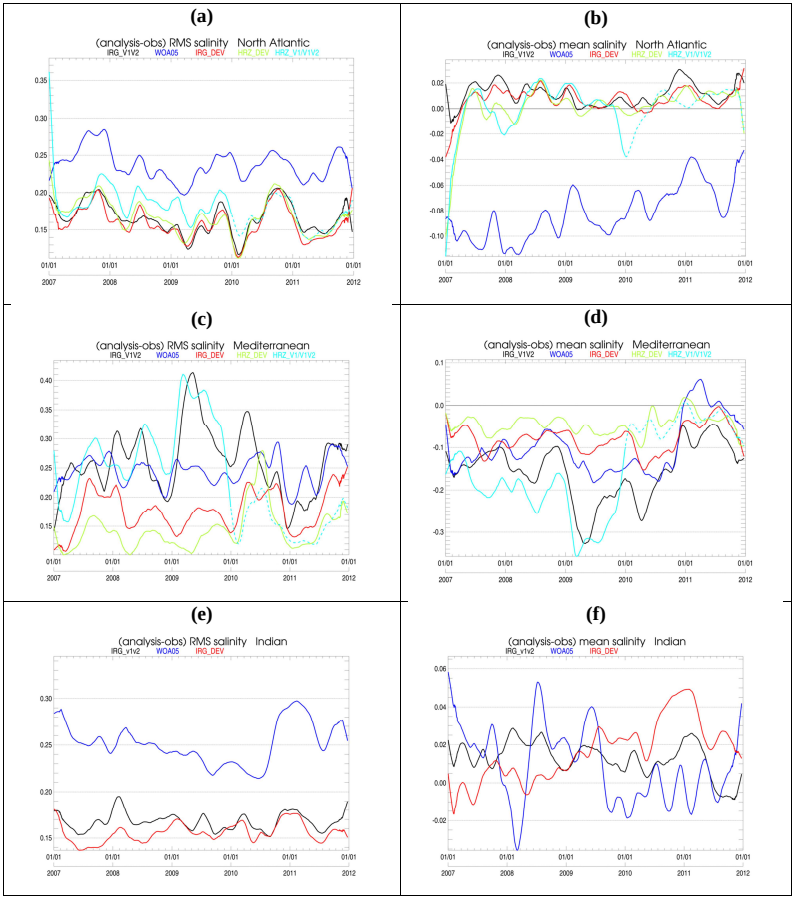

Fig. 6. Same as Fig. 5 but for salinity (psu).

OSD
9, 1123–1185, 2012

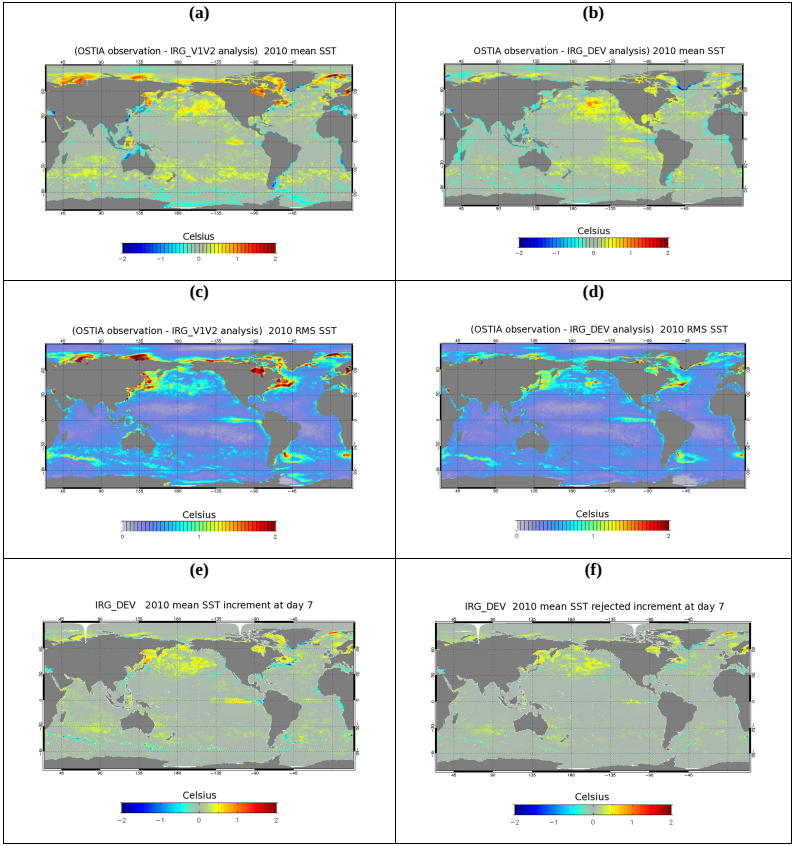

Fig. 7. 2010 SST (°C) mean (**a** and **b**) and RMS (**c** and **d**) differences (observation minus best analysis) between OSTIA observations and IRG daily average analyses co-localised with the observations. IRG_V1V2 system (**a** and **c**) is compared to IRG_DEV system (**b** and **d**). **(e)** 2010 mean SST increment injected into IRG_DEV system after 7 days. **(f)** 2010 mean SST rejected increment by the system after 7 days.

OSD
9, 1123–1185, 2012

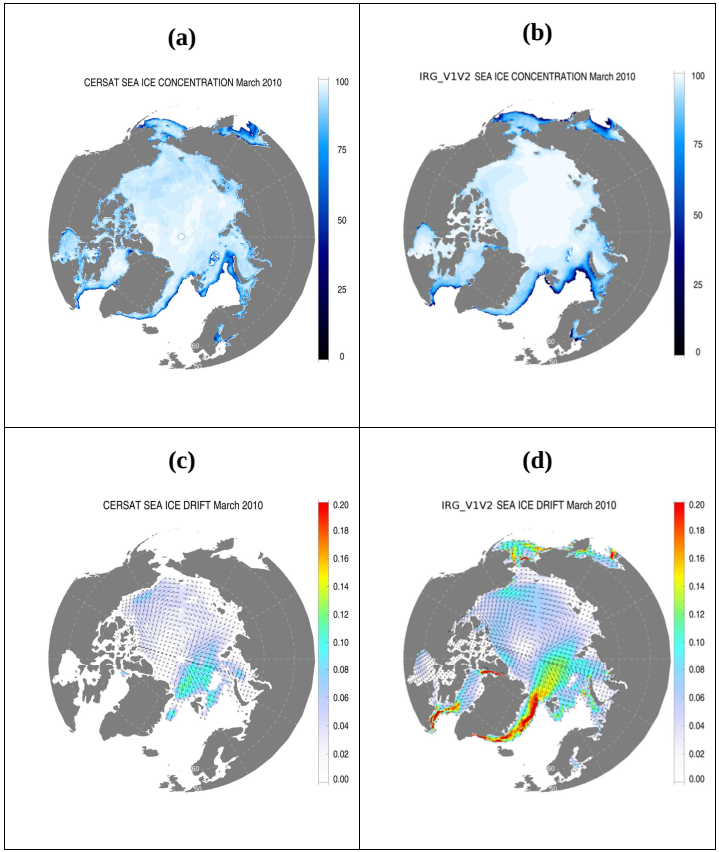

Fig. 8. Sea ice concentration (%) in the Arctic in March 2010: **(a)** from CERSAT satellite measurements, **(b)** from IRG_V1V2. Sea ice drift ($m\,s^{-1}$) in the Arctic in March 2010: **(c)** from CERSAT satellite measurements; **(d)** from IRG_V1V2.

OSD
9, 1123–1185, 2012

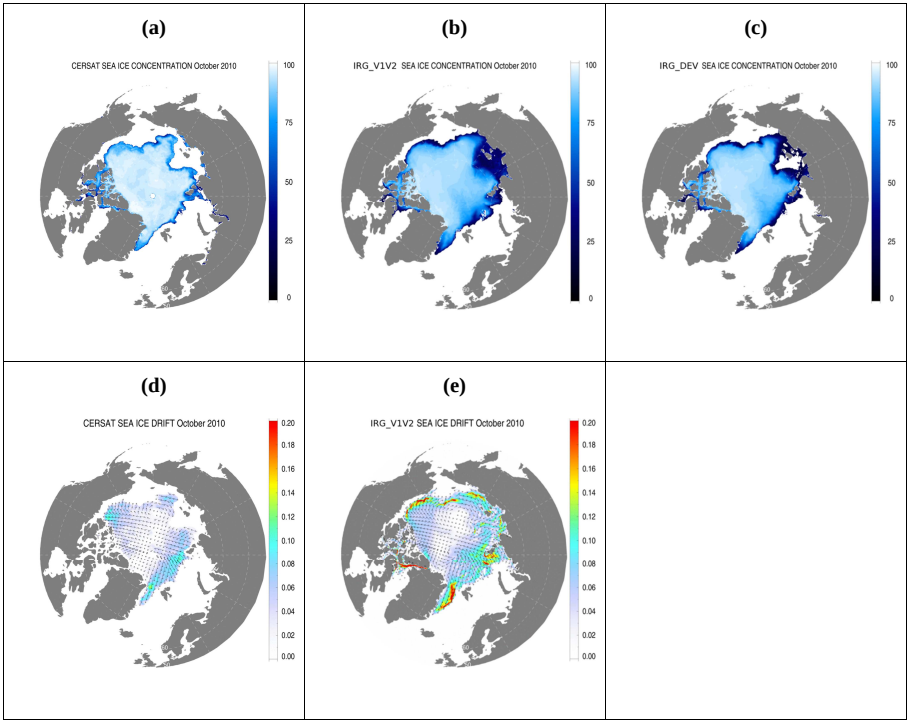

Fig. 9. Sea ice concentration (%) in the Arctic in October 2010: **(a)** from CERSAT satellite measurements, **(b)** from IRG_V1V2 , **(c)** from IRG_DEV. Sea ice drift ($m\,s^{-1}$) in the Arctic in October 2010: **(d)** from CERSAT satellite measurements; **(e)** from IRG_V1V2.

OSD
9, 1123–1185, 2012

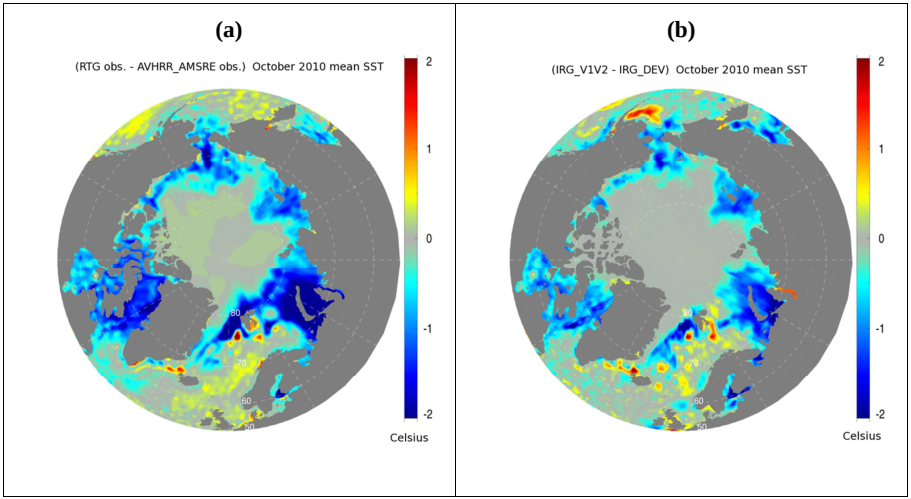

Fig. 10. Mean difference (°C) between assimilated SST products in IRG_V1V2 and IRG_DEV **(a)** and mean difference between IRG_V1V2 and IRG_DEV SST analyses themselves **(b)** in October 2010.

OSD
9, 1123–1185, 2012

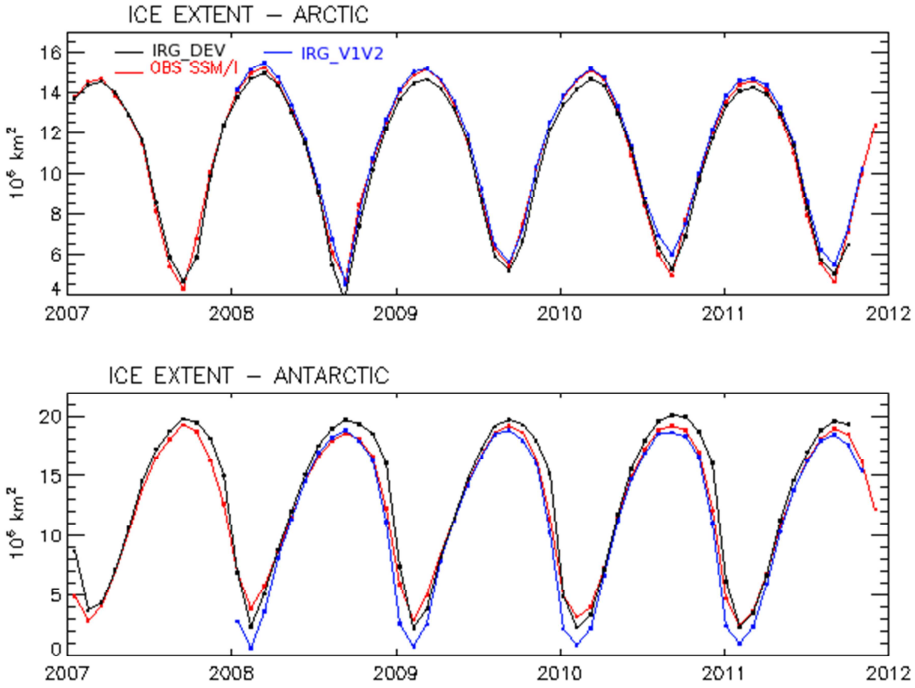

Fig. 11. Sea ice extent (10^6 km^2) in the Arctic (upper panel) and the Antarctic (lower panel) on the 2007–2011 period, from SSMI satellite measurements (red line) from IRG_V1V2 (blue line) and IRG_DEV (black line).

OSD
9, 1123–1185, 2012

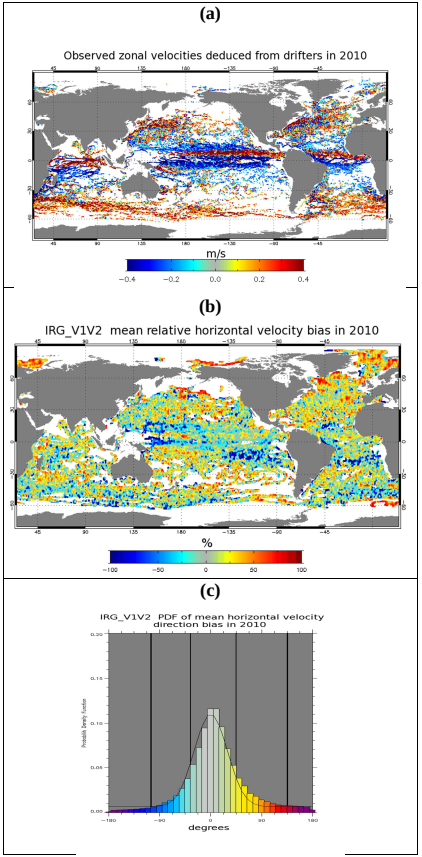

Fig. 12. Zonal velocity observations ($m\,s^{-1}$) with "Mercator Océan correction" (see text) deduced from all in situ Atlantic Oceanographic and Meteorological Laboratory drifters in 2010 **(a)**. Mean relative horizontal velocity bias (%) with respect to drifters in IRG_V1V2 **(b)**. Probability density function of the mean horizontal velocity direction bias (degrees) with respect to drifters in IRG_V1V2 **(c)**.

OSD
9, 1123–1185, 2012

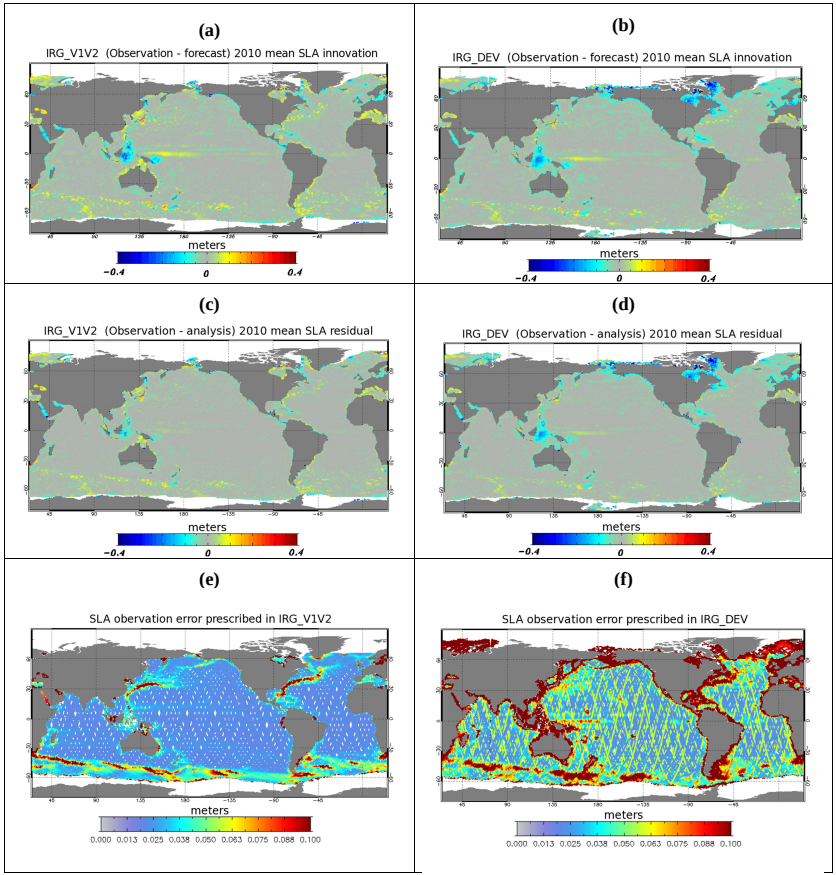

Fig. 13. Sea Level Anomaly SLA (m) innovations (**a** and **b**) and residuals (**c** and **d**) for the IRG_V1V2 (**a** and **c**) and IRG_DEV (**b** and **d**). Specified SLA observation error for IRG_V1V2 **(e)** and IRG_DEV **(f)**.

OSD
9, 1123–1185, 2012

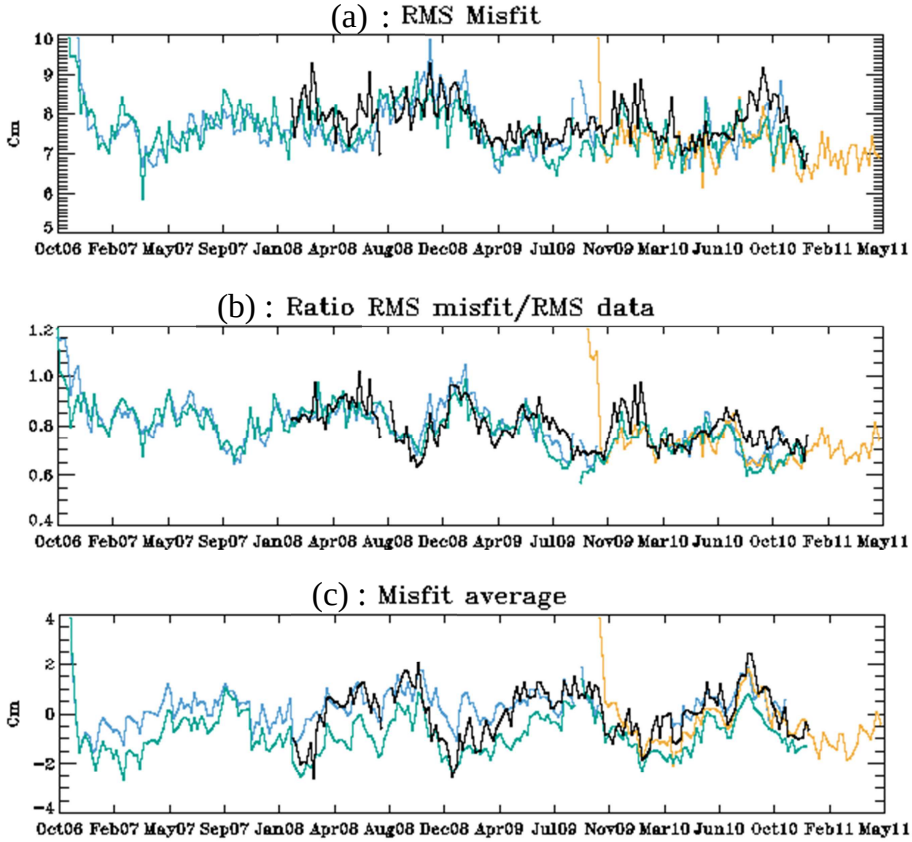

Fig. 14. Time evolution of Sea Level Anomaly SLA (m) data assimilation statistics averaged over the whole HRZ domain: RMS of innovations **(a)**; RMS of innovations divided by quadratic mean of SLA over the same region **(b)**; and average innovation **(c)**. The colours stand for different MyOcean versions of HRZ: HRZ_V0 (black), HRZ_V1 (blue), HRZ_V1V2 (orange) and HRZ_DEV (green).

OSD
9, 1123–1185, 2012

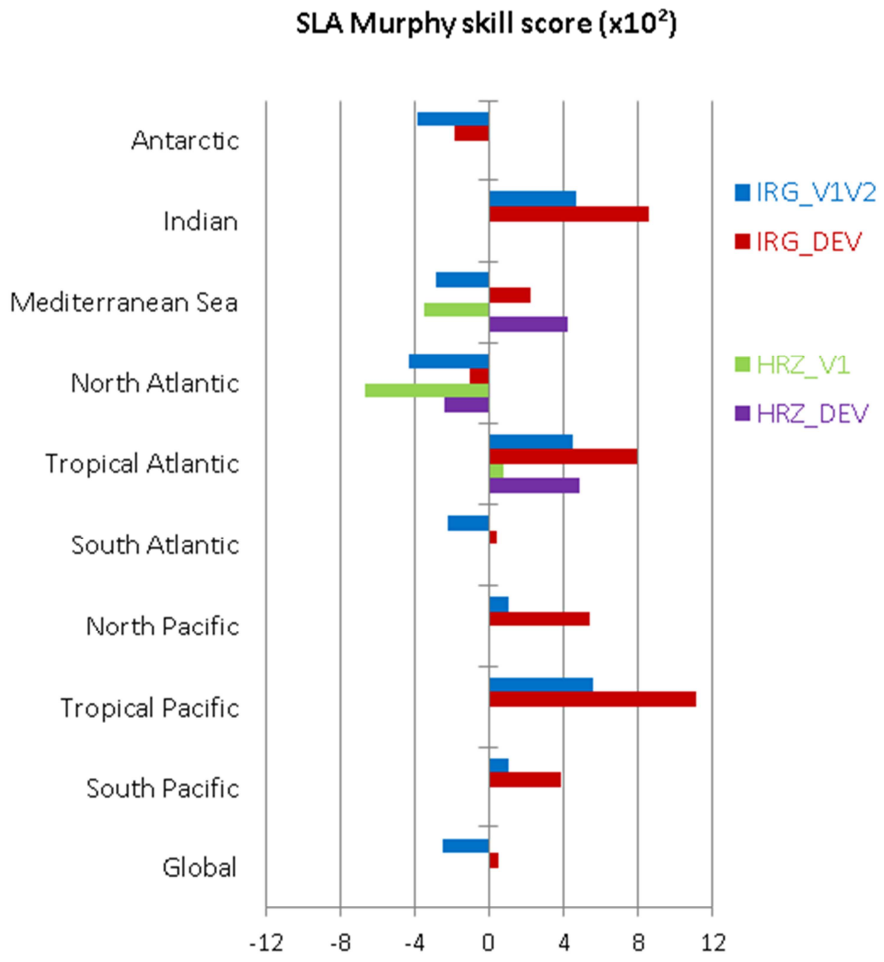

Fig. 15. Sea Level Anomaly Murphy skill score for the main GODAE regions.

OSD
9, 1123–1185, 2012

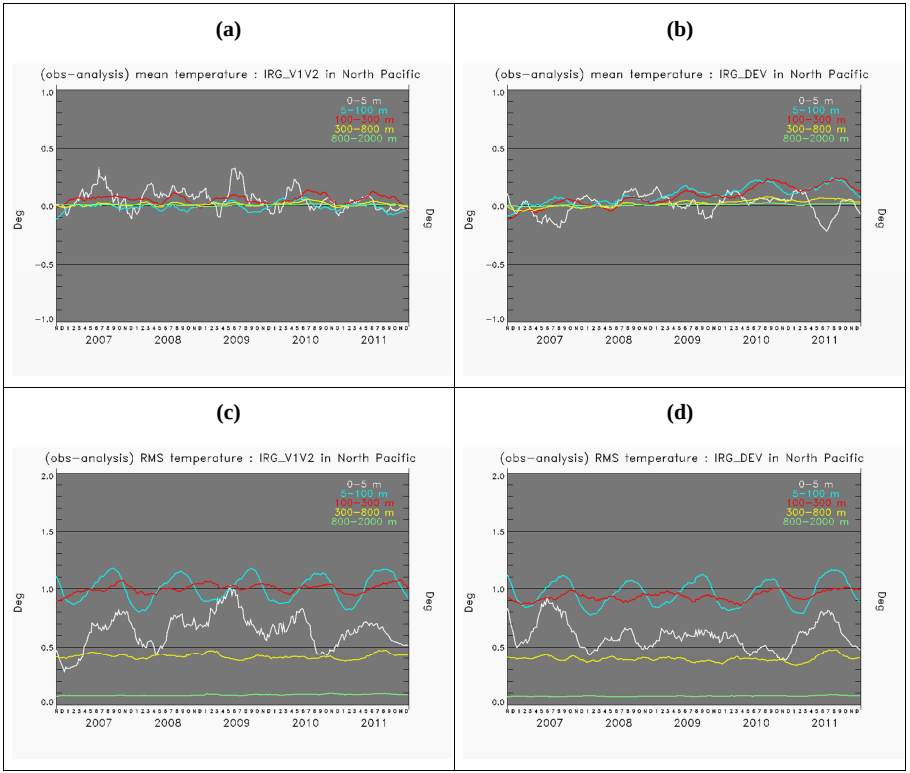

Fig. 16. Temperature data assimilation statistics in the North Pacific GODAE region, and for IRG_V1V2 (**a** and **c**) and IRG_DEV (**b** and **d**): Mean (**a** and **b**) and RMS (**c** and **d**) of temperature (°C) innovations (observation – forecast) computed in layers (0–5, 5–100, 100–300, 300–800, 800–2000) and as a function of time during the 2007–2011 period. For clarity, the time series were smoothed with a 60-day running mean.

OSD
9, 1123–1185, 2012

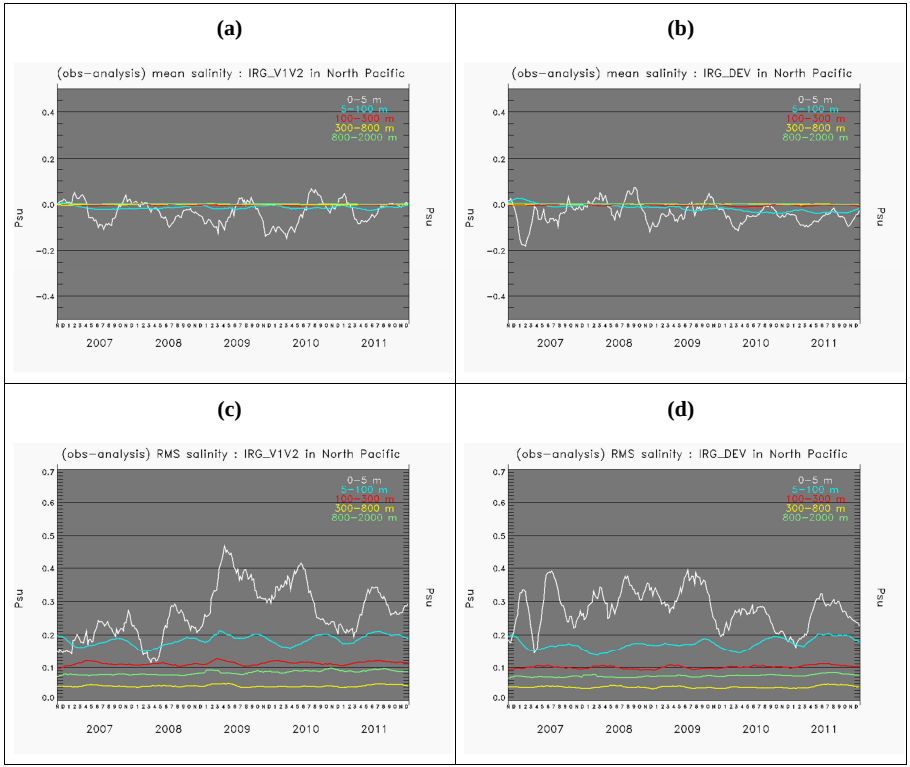

Fig. 17. Salinity data assimilation statistics in the North Pacific GODAE region, and for IRG_V1V2 (**a** and **c**) and IRG_DEV (**d** and **e**): Mean (**a** and **b**) and RMS (**c** and **d**) of salinity (psu) innovations (observation – forecast) computed in layers (0–5, 5–100, 100–300, 300–800, 800–2000) and as a function of time during the 2007–2011 period. For clarity, the time series were smoothed with a 60-day running mean.

OSD
9, 1123–1185, 2012

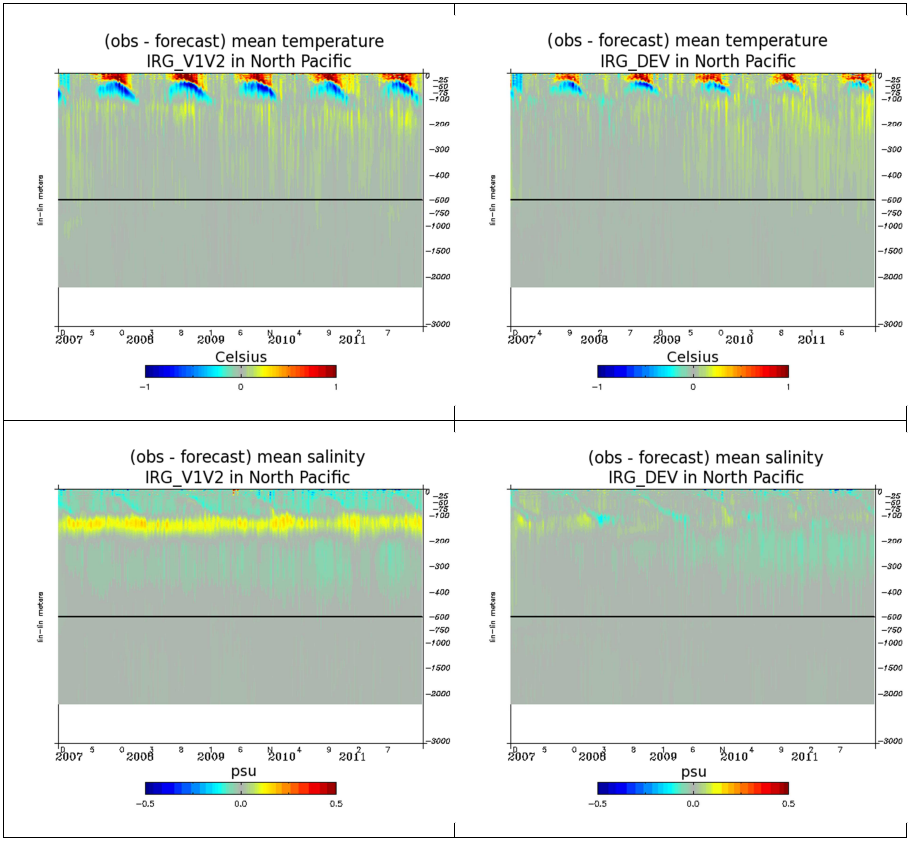

Fig. 18. Assimilation diagnostics with respect to the vertical temperature and salinity profiles over the period 2007–2011. Mean misfit between observations and model forecast for temperature (top panels) and salinity (low panels), in IRG_V1V2 (left panels) and IRG_DEV (right panels) systems.

OSD
9, 1123–1185, 2012

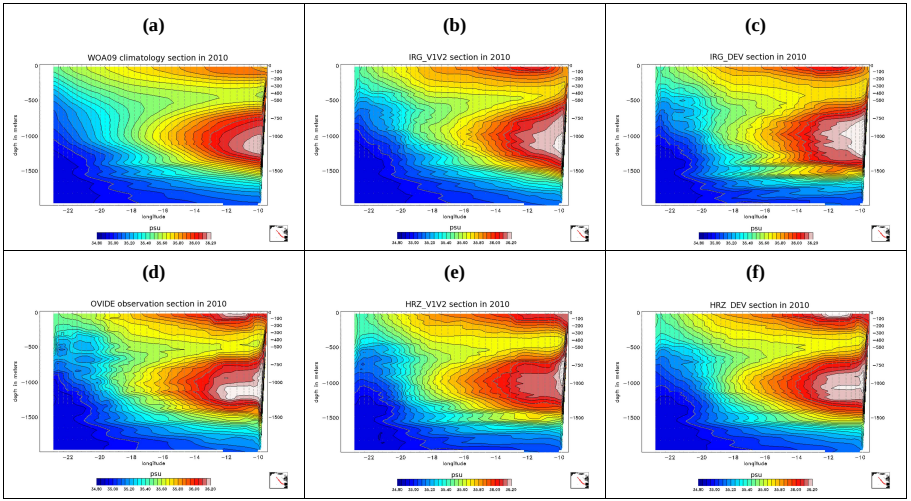

Fig. 19. Salinity (psu) along the OVIDE section in 2010 from WOA09 climatology **(a)**, IRG_V1V2 **(b)**, IRG_DEV **(c)**, in situ observations from CORIOLIS data base **(d)**, HRZ_V1V2 **(e)** and HRZ_DEV **(f)**. The contour interval is 0.05 psu.

OSD
9, 1123–1185, 2012

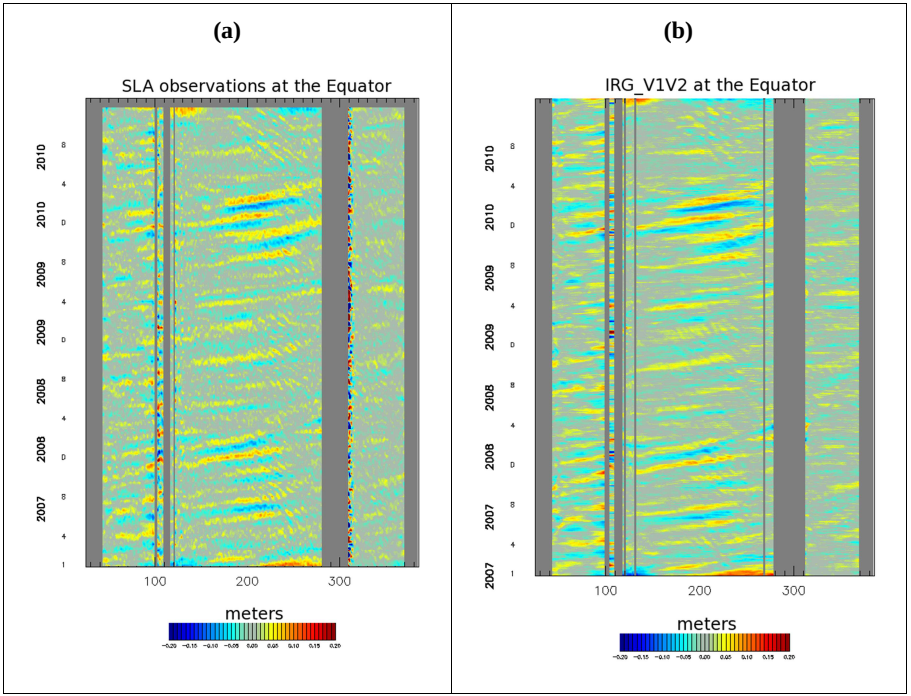

Fig. 20. SLA longitude time diagrams at the Equator over the world ocean. SLA from AVISO DUACS MyOcean SL TAC **(a)** and from IRG_V1V2 **(b)** are high pass filtered to keep fluctuations at periods shorter than 128 days.

OSD
9, 1123–1185, 2012

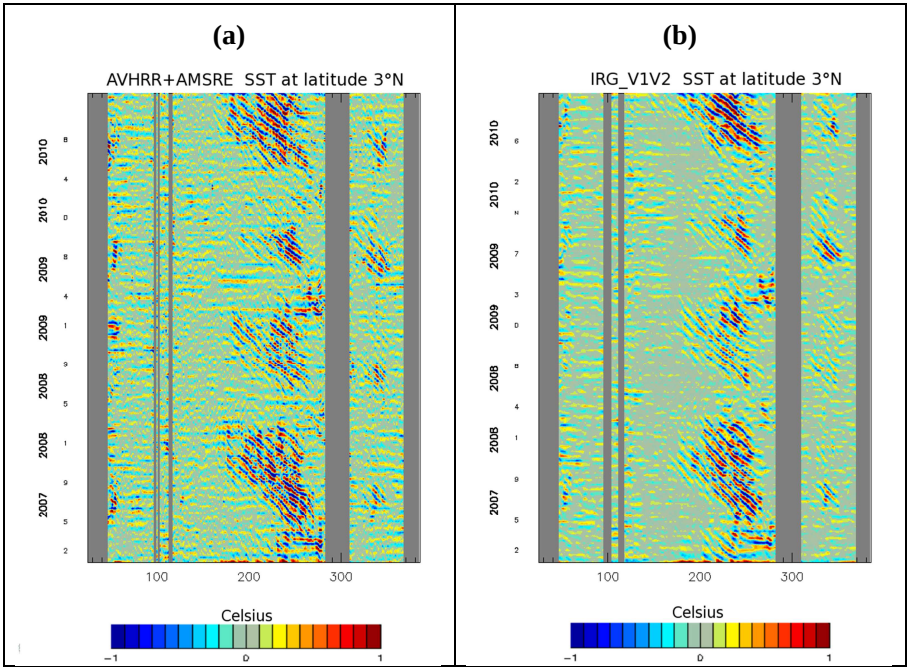

Fig. 21. SST longitude time diagrams at 3° N over the world ocean. SST from AVHRR + AMSRE **(a)**, IRG_V1V2 **(b)** are high pass filtered to keep fluctuations at periods shorter than 43 days.

OSD
9, 1123–1185, 2012

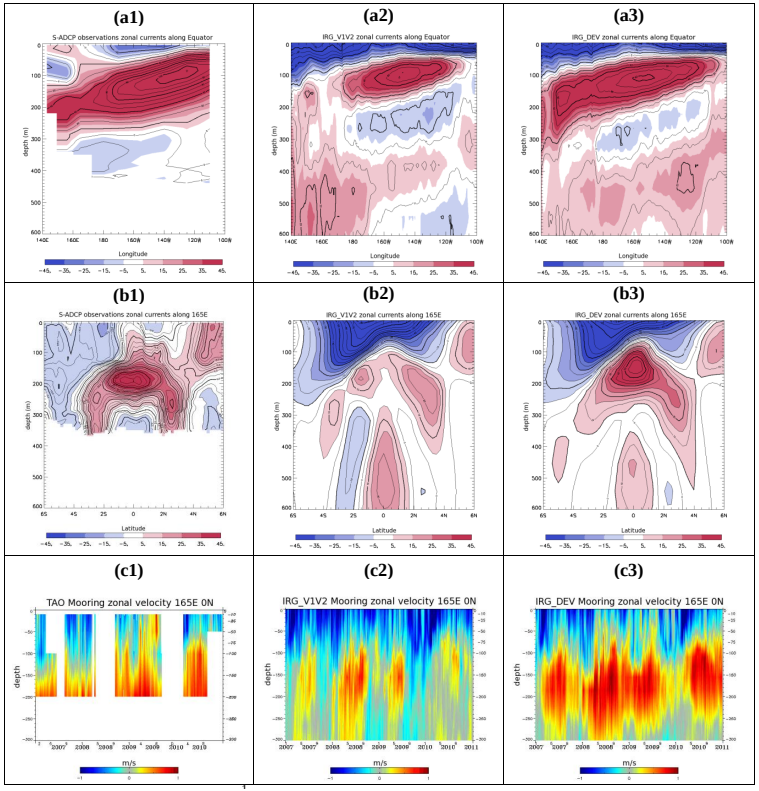

Fig. 22. Zonal velocity (cm s^{-1}) equatorial longitude-depth section **(a1, a2, a3)** and latitude-depth section at 165° E **(b1, b2, b3)** in the Pacific Ocean. Zonal velocities over depth and time at the 165° E/0° N TAO mooring for the 2007–2010 period **(c1, c2, c3)**. Zonal velocities come from IRG_V1V2 **(a2, b2, c2)** and IRG_DEV **(a3, b3, c3)** for the year 2010. Mean zonal sections of ADCP zonal currents come from Johnson et al. (2002) (**a1** and **b1**), and from the TAO ADCP measurements **(c1)**.

OSD
9, 1123–1185, 2012

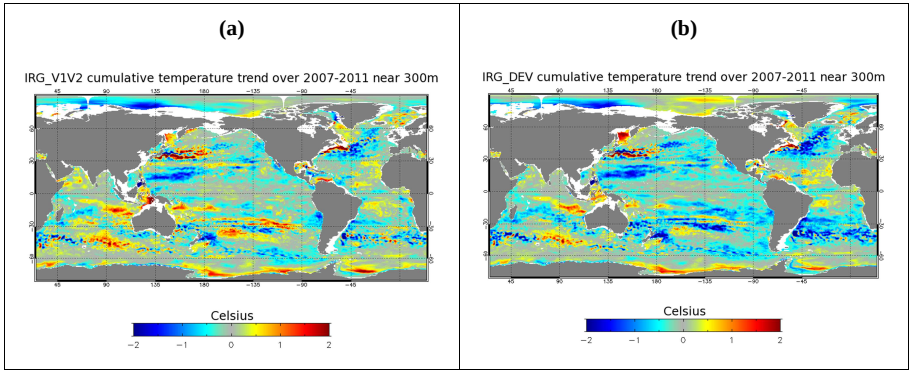

Fig. 23. Cumulative temperature trend (°C) over the 2007–2011 period for IRG_V1V2 **(a)** and IRG_DEV **(b)** systems.

OSD
9, 1123–1185, 2012

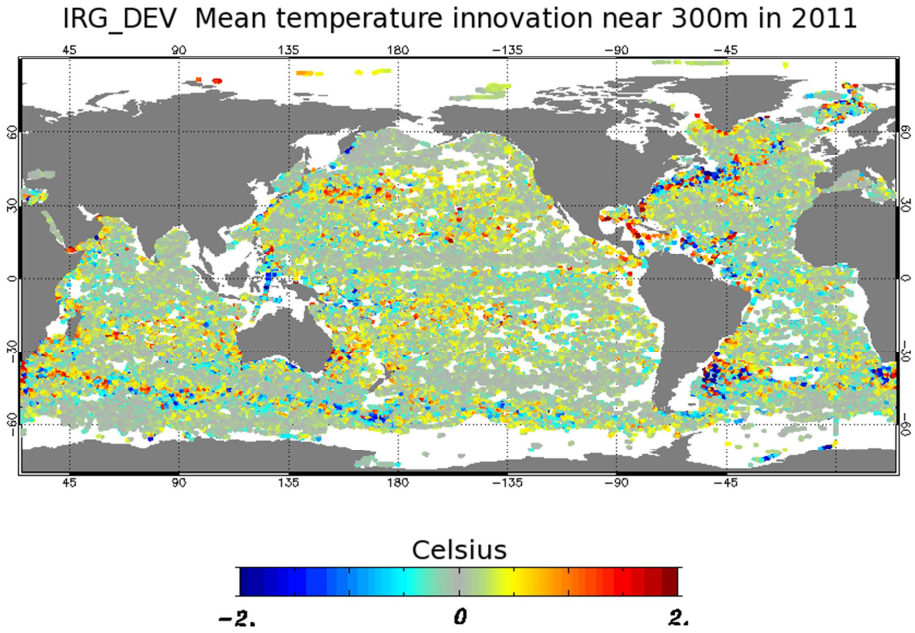

Fig. 24. Mean temperature innovation (°C) near 300 m in 2010 for IRG_DEV system.

OSD
9, 1123–1185, 2012

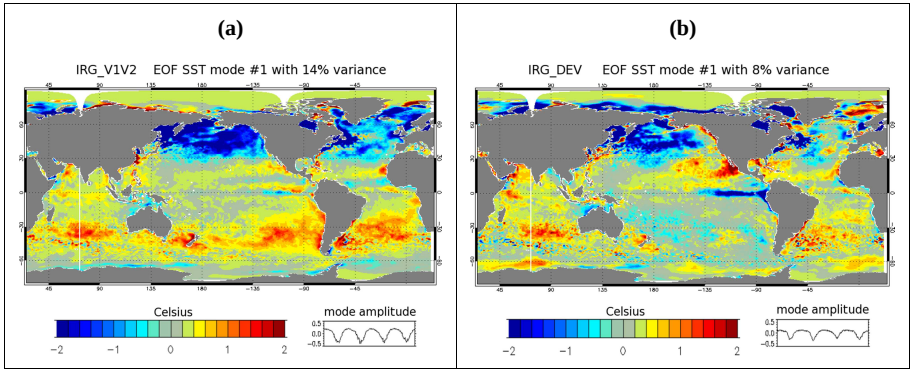

Fig. 25. 1st EOF of surface temperature increment (°C) over the 2007–2010 period for IRG_V1V2 **(a)** and IRG_DEV **(b)** systems.

OSD
9, 1123–1185, 2012